Aus der Neurochirurgischen Klinik und Poliklinik

Klinik der Ludwig-Maximilians-Universität München

Vorstand: Prof. Dr. med. Jörg-Christian Tonn

Intratumoral pericytes and non-canonical macrophages in glioma pathology

Dissertation

zum Erwerb des Doktorgrades der Medizin an

der Medizinischen Fakultät der

Ludwig-Maximilians-Universität zu München

vorgelegt von

Linzhi Cai

aus

Hubei, China

2020

Mit Genehmigung der Medizinischen Fakultät

der Universität München

Berichterstatter:	Prof. Dr. rer. nat. Rainer Glaß
Mitberichterstatter:	Prof. Dr. Gabriele Pöpperl
	PD. Dr. Markus Krumbholz
Mitbetreuung durch die promovierte Mitarbeiterin:	Dr. Sandra Ribes
Dekan:	Prof. Dr. med. dent. Reinhard Hickel
Tag der mündlichen Prüfung:	30.07.2020

LMU LUDWIG-MAXIMILIANS-UNIVERSITÄT MÜNCHEN

Dean's Office
Faculty of Medicine

MMRS MUNICH MEDICAL RESEARCH SCHOOL

Affidavit

CAI, LINZHI

Surname, first name

Street

Zip code, town

Country

I hereby declare, that the submitted thesis entitled

Intratumoral pericytes and non-canonical macrophages in glioma pathology

is my own work. I have only used the sources indicated and have not made unauthorised use of services of a third party. Where the work of others has been quoted or reproduced, the source is always given.

I further declare that the submitted thesis or parts thereof have not been presented as part of an examination degree to any other university.

Wuhan, 30.07.2020

Place, date

Cai, Linzhi

Signature doctoral candidate

Table of Contents

I. Abbreviations **4**

II. List of Figures **6**

III. List of Tables **7**

1. Introduction **8**

1.1 Glioblastoma 8

1.2 Subclassification of GBM and our glioma models 8

1.3 Tumor microenvironment and our mouse strains 9

1.4 Pericytes in the central nervous system (CNS) 10

1.5 Glioma-associated myeloid cells 11

1.6 Study aims 12

2. Materials **13**

2.1 Lab devices 13

2.2 Chemicals and reagents 14

2.3 Buffer formulations 15

2.4 Primary antibodies 16

2.5 Secondary antibodies 16

2.6 Other reagents for immunostaining 17

2.7 Commercial kits for immunostaining 17

2.8 Human glioblastoma specimens and tumor-free brain tissue 18

2.9 Glioma cell lines 18

2.10 Cell culture medium and reagents 18

2.11 Mouse strains 19

2.12 Drugs for animal experiments 19

2.13 Computer software 20

3. Methods **21**

3.1 Cell culture 21

3.2 Animal experimental models 21

3.2.1 Cre/lox-P system 21

3.2.2 Nestin::CreER^{T2}::R26-RFP (red fluorescent protein, RFP; nestin-reporter) mice 21

3.2.3 Other transgenic mouse models 22

3.2.4 Other animal experimental models 23

3.3 Animal experiments 23
3.3.1 Laboratory animal maintenance 23
3.3.2 Experimental schemes 24
3.3.3 Orthotopic glioma inoculation 24
3.3.4 Perfusion and tissue preparation 25
3.3.5 Cell isolation from mouse meninges and transplantation 26
3.4 Histology and immunohistochemistry 26
3.4.1 HE staining 26
3.4.2 Immunohistochemistry (IHC) 27
IHC staining with Mouse-on-mouse Kit 27
IHC staining for paraffin-embedded tissue 28
3.5 Microscopy 29
3.6 Cell number quantification 29
3.7 Tumor size quantification 30
3.8 Vascular analysis with Stereo-investigator 30
3.9 Statistical analysis 30

4. Results 31

4.1 Vascular and avascular RFP expressing cells in the GBM microenvironment of nestin-reporter models 31
4.2 Vascular RFP expressing cells are pericytes 33
4.3 Avascular RFP expressing cells are tumor-associated cells with a myeloid-like expression profile (TAMEP) 35
4.4 Sox2 is expressed in avascular RFP expressing cells, but not in vascular RFP expressing cells 38
4.5 Sox2 expression in TAMEP 40
4.6 Sox2/RFP co-expressing cells are SOX2-dependent and required for the generation of TAMEP 42
4.7 S2-MP/TAMEP do not originate from BM-derived cells 45
4.8 S2-MP/TAMEP express the myeloid transcription factor Pu.1 47
4.9 SOX2/PU.1 co-labelled cells in murine and human GBM 48
4.10 S2-MP/TAMEP contribute to tumor angiogenesis by promoting vessel branching in the early phase of tumorigenesis 50
4.11 S2-MP/TAMEP control GBM expansion 53

4.12 S2-MP/TAMEP and RFP expressing pericytes derived from the meninges.... 54

5. Discussion 58

6. Summary 63

Zusammenfassung 65

7. References 67

8. Acknowledgements 73

I. Abbreviations

αSMA	α-smooth muscle actin
BBB	Blood-brain barrier
CCR2	C-C Motif Chemokine Receptor 2
CDKN2a	Cyclin-dependent Kinase Inhibitor 2A
CNS	Central nervous system
Cre	Cyclisation recombination
CX3CR1	C-X3-C Motif Chemokine Receptor 1
DAPI	4,6-diamidino-2-phenylindole
DMEM	Dulbecco's MEM
DPO	days post operation
EGFRvIII	Epidermal Growth Factor Receptor Variant III
ER	Estrogen receptor
Flt3	FMS-like tyrosine kinase 3
GFP	Green fluorescent protein
GSC	Glioma stem cell
HE staining	Hematoxylin-eosin staining
hGBM	Human glioblastoma
HOPE	Hepes glutamic acid buffer mediated organic solvent protection effect
IDH	Isocitrate dehydrogenase
IDTA	Cre-inducible diphtheria toxin A
IHC	Immunohistochemistry
i.p.	Intraperitoneal
KI	Knock-in
KO	Knock-out
Lox-P	Locus of crossing [x-ing]-over of bacteriophage P1
LSL	lox-STOP-lox cassette
Nestin-reporter	Nestin:: $CreER^{T2}$, Ai9-tdTomato
NOS	not otherwise specified

Abbreviations

NPC	Neural precursor cell
PBS	Phosphate buffered saline
PDGF-B	Platelet-derived growth factor subunit B
PDGFR-β	Platelet-derived growth factor receptor β
Pu.1	Transcription factor Pu.1 (SPI1)
RFP	Red fluorescent protein
Sox2	SRY (sex determining region Y)-box 2
$SOX2^{fl/fl}$	lox-flanked SOX2 gene
SOX2-KO	$SOX2^{fl/fl}$ Nestin-reporter mouse (SOX2 conditional knock out)
S2-MP	SOX2-dependent cells required for the generation of TAMEP
TAM	Tumor-associated myeloid cell
TAMEP	tumor-associated cells with a myeloid-like expression profile
TP53	Tumor protein P53
vWF	von Willebrand factor

II. List of Figures

Figure-1. Glioblastoma microenvironment..... 10
Figure-2. Function and dysfunction of pericytes in the CNS. 11
Figure-3. The mechanism of RFP expression in traced cells in nestin-reporter models 22
Figure-4. Animal experimental schemes..... 24
Figure-5. Orthotopic glioma inoculation 25
Figure-6. Vascular and avascular RFP expressing cells in the GBM microenvironment of nestin-reporter models 32
Figure-7. Vascular RFP expressing cells are pericytes 34
Figure-8. Avascular RFP expressing cells are TAMEP..... 37
Figure-9. Sox2 is expressed in avascular RFP expressing cells, but not in vascular RFP expressing cells 39
Figure-10. Sox2 expression in TAMEP..... 41
Figure-11. Sox2/RFP double-postive cells are S2-MP 44
Figure-12. S2-MP/ TAMEP do not originate from BM-derived cells 46
Figure-13. S2-MP/TAMEP express the myeloid transcriptional factor Pu.1..... 47
Figure-14. SOX2/PU.1 double-labelled cells in murine and human GBM 49
Figure-15. S2-MP/TAMEP contribute to tumor angiogenesis by promoting vessel branching in the early phase of tumorigenesis..... 52
Figure-16. S2-MP/TAMEP control GBM expansion..... 54
Figure-17. S2-MP/TAMEP and RFP expressing pericytes originated from cells on meninges 55
Figure-18. The transplantation of meninges cells from newborn Cx3cr1$^{GFP/+}$; nestin-reporter mice to the GBM of athymic nude mice 56
Figure-19. A summary of the function of S2-MP/ TAMEP 61

III. List of Tables

Table-1. *Lab devices* 13
Table-2. *Chemicals and reagents* 14
Table-3. *Buffer formulations* 15
Table-4. *Primary antibodies* 16
Table-5. *Secondary antibodies* 16
Table-6. *Other reagents for immunostaining* 17
Table-7. *Commercial kits for immunostaining* 17
Table-8. *Glioma cell lines* 18
Table-9. *Cell culture medium and reagents* 18
Table-10. *Mouse strains* 19
Table-11. *Drugs for animal experiments* 19
Table-12. *Computer software* 20
Table-13. *Molecular markers of vascular RFP expressing cells* 33
Table-14. *Molecular markers of avascular RFP expressing cells* 36

1. Introduction

1.1 Glioblastoma

Glioblastoma (GBM) is the most frequent primary tumor in the human adult central nervous system[1]. The overall annual incidence of GBM is 3 per 100,000 population, and it is most abundant in 40+ adults[2]. Due to its high malignancy and heterogeneity, the prognosis is poor and has not been significantly improved despite new developments in diagnostic methods and treatment strategies[1]. Medium survival is only 14-16 months despite multidisciplinary treatments[3].

Until recently, the diagnosis of GBM was largely based on neurological symptoms, neuroimaging, and histological confirmation[1]. The histological diagnosis is still the 'gold standard'[4]. Usually, GBM presents with neovascularization and necrosis, which are supposed to be distinguishing histopathological features of GBM[1]. In the last two decades, diverse genetic and molecular aberrations of GBM have been revealed[5-9]. Some of them, which include isocitrate dehydrogenase mutation, 1p/19q codeletion, histone H3-K27M mutation and O^6-methylguanine DNA methyltransferase (MGM promoter methylation[5,10], have been used for improving the prognosis and selection of chemotherapy regimens. With the 2016 classification of World Health Organization of Tumors of CNS, GBM is classified into IDH mutant, IDH wildtype and IDH not otherwise specified, which started a molecular era for the diagnosis and treatment of GBM in clinic[11,12].

In this new era of precise medicine, the diagnosis of GBM is mainly based on molecular features[4,12]. For newly diagnosed GBM, the standard treatment is maximal surgical removal of the tumor followed by the Stupp regimen[13] which describes a strategy for concomitant chemoradiotherapy[1,4,13].

1.2 Subclassification of GBM and our glioma models

The molecular heterogeneity of GBM maybe one reason for the poor prognosis after radiotherapy and chemotherapy[5,14-17]. With the analysis of molecular genetic data from The Cancer Genome Atlas [9] Research Network, GBM is sub-grouped into three subtypes: classical, mesenchymal and proneural[5].

Based on the genomic expression features for each subtype, gene-modified mouse models are generated by manipulating targeted genes in neural precursor cells (NPC)[18]: Mouse GBM cells of the "classical" subtype are obtained by forced expression of EGFRvIII into $CDKN2a^{KO}$ NPC, while the proneural mouse GBM cells comprise $TP53^{KO}$_$PDGFb^{KI}$ NPC. Some human glioma cell lines from different subtypes were obtained for this study, such as proneural GBM cells NCH644, GBM cells GBM14 and classical GBM cells GBM2. All these glioma cells were instrumental for this study to explore tumor microenvironments in different genetic subtypes of murine and human GBM.

1.3 Tumor microenvironment and our mouse strains.

Glioblastoma multiforme consist of not only glioma cells but also extracellular matrix and stromal cells[14,15]. Stromal cells include neurons, astrocytes, endothelial cells, pericytes, immune cells, microglia and macrophages (Fig. 1)[14,19]. In the tumorigenesis, glioma cells activate, recruit and manipulate non-tumor cells from the brain parenchyma or blood to support tumor progression[14,20-23]. Similar to the genetic and molecular heterogeneity of glioblastoma cells, the heterogeneity of these tumor-associated cells also contributes to the heterogeneity of GBM[22-24]. As these stromal cells are crucial for the intratumor heterogeneity[19,24], tumor angiogenesis[25], immune escape[26,27] and resistance to radiochemotherapy[14], it is reasonable to target stromal cells for developing new therapies of GBM.

Some stem- and progenitor cells are also attracted to the border of GBM and participate in tumor pathology, such as NPC[28] and oligodendrocyte progenitor cells (OPC)[29]. NPC can reduce glioma expansion by release of reactive lipids[28]. OPC can promote to the invasion[29] and neovascularization[30] of GBM. Mesenchymal stem cells (MSC) also play roles in tumorigenesis[31,32.] However, it is still unclear if any other population of resident progenitor cells contributes to GBM pathology in the tumor environment.

Transgenic mice carrying the Cre-loxP system are commonly applied to trace progenitor cells and their daughter cells[22]. Using a lineage- tracing transgenic model (nestin-$creER^{T2}$::R26-RFP, also termed as nestin-reporter) in this study, we monitor intratumoral pericytes, non-canonical tumor-associated myeloid cells and their progenitors in the GBM microenvironment.

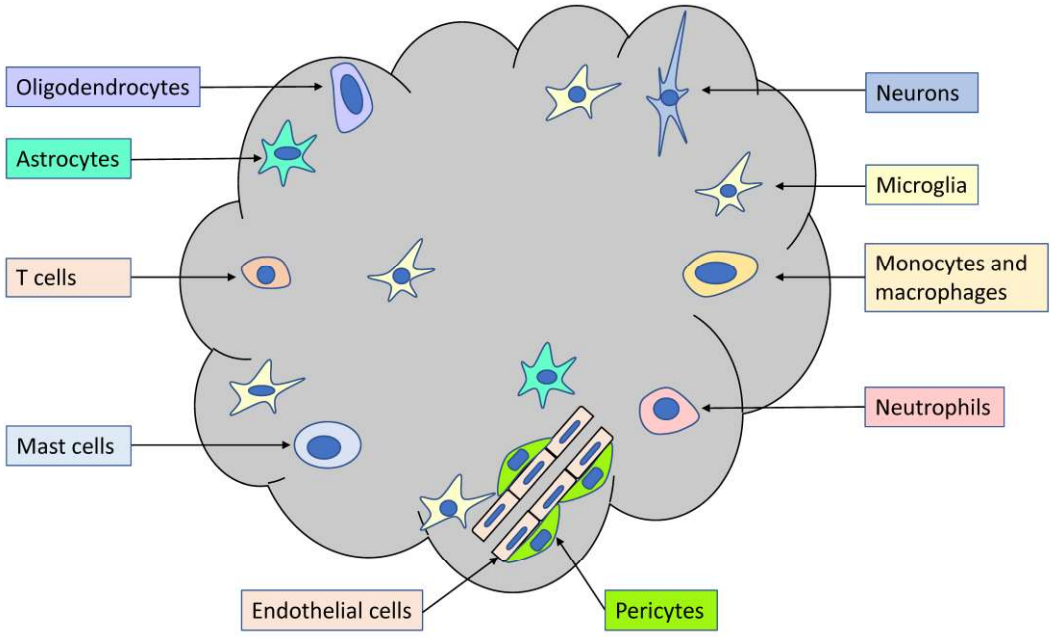

Figure-1. Glioblastoma microenvironment. In the microenvironment of GBM, several types of stromal cells including neurons, astrocytes, oligodendrocytes, endothelial cells, pericytes, immune cells (T cells, B cells, mast cells, neutrophils), microglia and macrophages are related to tumor pathology[19].

1.4 Pericytes in the central nervous system

Pericytes are vascular mural cells, which are located at the endothelial basement membrane[33,34]. Currently, the identification of pericytes is based on their location, morphology and molecular markers[34,35]. Anatomically, pericytes envelop and stretch along the capillary[35]. Pericyte markers include platelet-derived growth factor receptor-β (PDGFRβ) [36], α-smooth muscle actin[37], desmin[38], aminopeptidases A and N (CD13)[39] as well as the transmembrane chondroitin sulfate proteoglycan NG2[40]. Pericytes can be subclassified into diverse subpopulations based on their different locations and functions[41].

Data from animal experiments show that neuroectoderm-derived neural crest cells generate pericytes of the forebrain, and mesoderm-derived mesenchymal stem cells give rise to pericytes of the brainstem and spinal cord [42-44]. During the early postnatal periods and embryogenesis, pericytes are generated in brain parenchyma and they play roles in angiogenesis [45,46]. During brain ischemia-induced angiogenesis, bone marrow-derived cells can also differentiate into pericytes[47].

Pericytes play key roles in maintaining the structure and function of the neurovascular unit [33]. Physiologically, pericytes keep the integrity of the blood-brain barrier (BBB), control the BBB permeability for molecular exchange and immune cell penetration, participate in angiogenesis by recruiting endothelial cells and regulate cerebral blood flow. Pericytes also have multi-potency similar to mesenchymal stem cells [33-35]. The dysfunction of pericytes can lead to a range of neuropathological disorders [34], such as the breakdown of BBB, aberrant angiogenesis and cerebral blood flow dysfunction (Fig. 2) [48]. Pericytes participate in many neuropathological processes [48], such as stroke [49], epilepsy [50], spinal cord injury [51], Alzheimer's diseases [52] and glioma [48].

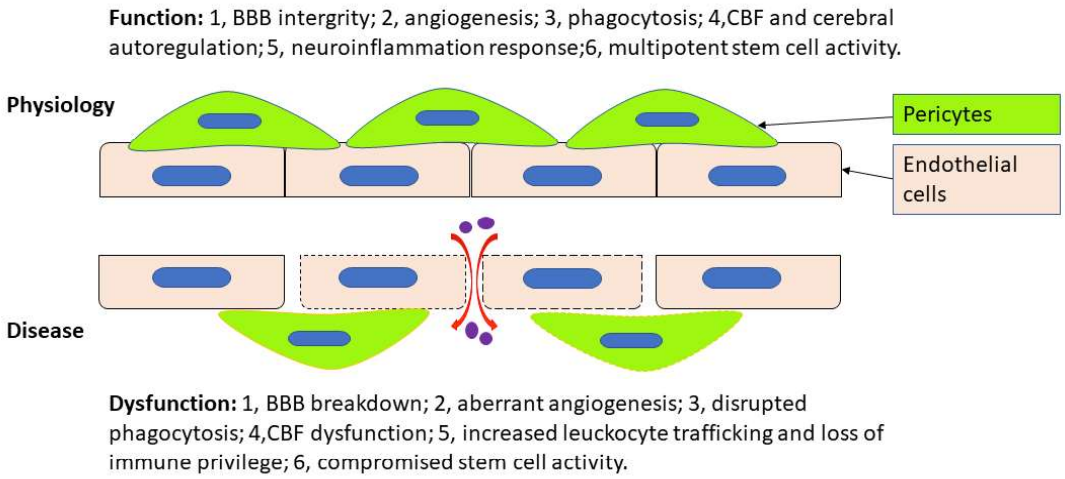

Figure-2. Function and dysfunction of pericytes in the CNS[34,48]. Physiologically, CNS pericytes maintain the integrity of the blood-brain barrier (BBB), control the permeability and regulate cerebral blood flow, CNS pericytes also contribute to angiogenesis, phagocytosis and immune response. Also, CNS pericytes have multipotent stem cell activity. Pathologically, the dysfunction of pericytes result in the BBB breakdown, aberrant angiogenesis, disrupted phagocytosis, cerebral blood flow dysfunction, increased leukocyte trafficking and loss of immune privilege and compromised stem cell activity.

In brain tumors, pericytes contribute to tumor angiogenesis, support tumor cells growth, and regulate tumor microenvironment [53]. Sun et al. reported that pericytes contributed to the malformed microvasculature of GBM [54]. It was also reported that pericytes played a key role in the blood-tumor barrier[48]. Pericytes could be promising targets for reducing chemotherapy resistance[48].

1.5 Glioma-associated myeloid cells

In the CNS, myeloid cells (microglia and macrophages) contribute to maintaining the CNS homeostasis and participate in pathological processes of many CNS diseases [55-57].

It is believed that all CNS myeloid cells share molecular markers Iba1, F4/80, CD11b and Cx3cr1[58]. As introduced above, GBM are a set of highly heterogeneous malignant glial tumors with a large population of stromal cells in the tumor environment[5,19]. Tumor associated myeloidc cells (TAM) originate from the proliferative expansion of parenchymal microglia ($CD11b^{+}/CD45^{low}$) and invading monocyte ($CD11b^{+}/CD45^{high}$) from hematopoietic stem cells[59,60]. Monocyte-derived macrophages make up the majority of TAM[22] and can be visulised e.g. in $CCR2^{GFP}$ transgenic mice[23].

In general, TAM contribute to GBM growth and invasion [20] by release of stress-inducible protein 1 (STI1), epidermal growth factor (EGF), transforming growth factor-β (TGF-β), interleukin-6 (IL6), as well as other cytokines [61-64]. Also, TAM contribute to immune suppression by expressing IL-6, IL-10 and TGF-β in GBM [22]. TAM participate in all processes of tumor neo-vascularisation, from early tip cell-guided sprouting and vessel branching to later vascular stabilisation[25]. TAM also promote tumor angiogenesis by interacting with endothelial cells and vascular mural cells through the release of some alternative pro-angiogenic factors, like IL-6, IL-10 [22,25]. Brandenburg et al. report that the resident microglia control tumor angiogenesis and promote tumor expansion[65]. Targeting TAM could bring a new anti-angiogenesis therapy for GBM patients[21].

1.6 Study aims

Using a transgenic lineage-tracing model (nestin-reporter mice), we traced a small population of avascular red fluorescent protein-expressing cells (termed as avascular RFP expressing cells or avascular RFP+ cells) and vascular RFP expressing cells in the GBM microenvironment. In this study,we ask following questions:

a) What are vascular/avascular RFP expressing cells?
b) Are vascular/avascular RFP expressing cells pathologically important? What are their functions in the GBM microenvironment?
c) Do they exist in other mouse models and human GBM?
d) Where do vascular/avascular RFP expressing cells originate from?

2. Materials

2.1 Lab devices

Table-1. Lab devices

Equipment/ Device	Company
Clean Bench	Thermo Fisher Scientific, Waltham, MA, USA
CO_2 incubators	BINDER, Tuttlingen, Germany
Water bath	Memmert GmbH + Co. KG, Schwabach, Germany
Centrifuge 5415R	Eppendorf AG, Hamburg, Germany
Fridge (4°C, -20°C, -80°C)	LIEBHERR, Bulle, Switzerland
Sea Star Shaker	Biozyme Scientific GmbH, Oldendorf, Germany
MS2 mini shaker	IKA, Staufen, Germany
Digital Vortex mixer	VWR, Radnor, Pennsylvania, USA
Stereotactic Frame	Stoelting Co., Wood Dale, IL, USA
Microliter syringe (1 µl)	Hamilton Company, Reno, NV, USA
Surgical instruments	Medizinisches Lager Klinikum der Universität München, Munich, Germany
DOSE IT peristaltic pump	Integra Biosciences AG, Zizers, Switzerland
Ethibond excel (5-0)	Ethicon, Germany
Perfusion system Dose IT P910	Integra Biosciences
Magnetic Hotplate Stirrer VMS-C7-2	VWR International GmbH, Darmstadt, Germany
WTW Multical bench pH Meter (pH 526)	Sigma-Aldrich, Saint Louis, MO, USA
Superfrost Ultra Plus microscope slides	Thermo Fisher Scientific, Waltham, MA, USA
Slide 2003 Microtome	Pfm Medical, Cologne, Germany
Menzel microscope coverslips (24 x 50mm)	Gerhard Menzel GmbH, Braunschweig, Germany
Dako Pen	Dako Germany, Hamburg, Germany
Parafilm	Biozym Scientific GmbH, Hessisch Oldendorf, Germany
Drying block	Whatman GmbH, Dassel, Germany
Becherglas (250, 500, 1000 ml)	DURAN Group GmbH, Wertheim, Germany
Costar Stripettes (5, 10 and 25 ml)	Corning Incorporated, Corning, NY, USA
Spritzen BD Discardit II (5 and 10 ml)	Becton Dickinson, Franklin Lakes, NJ, USA
Pipet Boy Comfort	Integra Biosciences AG, Zizers, Switzerland
Pipettes (0-10, 20-200, 100-1000 µl)	Eppendorf AG, Hamburg, Deutschland
Eppendorf tubes (0.5, 1 and 2 ml)	Eppendorf AG, Hamburg, Germany
Falcon tubes (15 and 50 ml)	VWR International GmbH, Darmstadt, Germany
Pipet-Aid XP2	Drummond Scientific Company, Pennsylvania, United States
Pipette Tip (0-10, 20-200, 100-1000 µl)	Gilson S.A.S, Villiers-le-Bel, France

Tissue Culture Test plate (12, 24, 96 well	TPP Techno Plastic Products AG, Trasadingen, Switzerland
Tissue culture flasks (T25, T75, T150)	TPP Techno Plastic Products AG, Trasadingen, Switzerland
Centrifuge Tube (15, 50 ml)	TPP Techno Plastic Products AG, Trasadingen, Switzerland
STRIPETTE (5, 10, 25, 50 ml)	Corning, New York, USA
Safe-Lock Tubes 1.5 ml	Eppendorf AG, Hamburg, Germany
Greiner Cryo.S™ vials	Greiner Bio-one GmbH, Frickenhausen, Germany
Axio Observer A1 inverse fluorescence microscope	Carl Zeiss Microscopy GmbH, Jena, Germany
Axioskop 2 light microscope	Carl Zeiss Microscopy GmbH, Jena, Germany
Axiovert 135 TV fluorescence microscope	Carl Zeiss Microscopy GmbH, Jena, Germany
Axiovert 25 fluorescence microscope	Carl Zeiss Microscopy GmbH, Jena, Germany
BMS D1-223A light microscope	Breukoven b. v., Capelle aan den Ijssel, Netherlands
Leica confocal laser microscope SP8 Upright Confocal 405/WLL Phys Stand Malpighi	Leica Microsystems Vertrieb GmbH, Wetzlar, Germany

2.2 Chemicals and reagents

Table-2. Chemicals and Reagents

Chemical/ reagent	**Company**
Isopropanol #9866.6	Roche Diagnostics GmbH, Rotkreuz, Switzerland
Aceton #5025.1	Roche Diagnostics GmbH, Rotkreuz, Switzerland
Citric acid # C0759	Sigma-Aldrich, Saint Louis, MO, USA
tri-Natriumcitrat- Dihydrate	Roche Diagnostics GmbH, Rotkreuz, Switzerland
Sodium Tetraborate decahydrate	Sigma-Aldrich, Saint Louis, MO, USA
Roti® Histol	Carl Roth GmbH + Co. KG, Karlsruhe, Germany
Eosin G-solution 0.5%	Carl Roth GmbH + Co. KG, Karlsruhe, Germany
Meyer's Hemalaun	Carl Roth GmbH + Co. KG, Karlsruhe, Germany
EtOH 100%	Apotheke Klinikum der Universität München, Munich, Germany
EtOH 70%	Apotheke Klinikum der Universität München, Munich, Germany
EtOH 96%	Apotheke Klinikum der Universität München, Munich, Germany
Glycerol	Sigma-Aldrich, Saint Louis, MO, USA
Ethylene glycol	Sigma-Aldrich, Saint Louis, MO, USA
PFA	Sigma-Aldrich, Saint Louis, MO, USA

Sucrose	Sigma-Aldrich, Saint Louis, MO, USA
PBS	Apotheke Klinikum der Universität München, Munich
NaOH	Sigma-Aldrich, Saint Louis, MO, USA
HCl	Sigma-Aldrich, Saint Louis, MO, USA
Na2HPO4	Sigma-Aldrich, Saint Louis, MO, USA
NaH2PO4	Sigma-Aldrich, Saint Louis, MO, USA
Aqua ad injectabilia	B. Braun Melsungen AG, Melsungen, Germany
Triton X-100	Roche Diagnostics GmbH, Rotkreuz, Switzerland
Tween-20	Sigma-Aldrich, Saint Louis, MO, USA
Dako Antibody Diluent #S3002	Dako Germany, Hamburg, Germany
Dako Biotinylated link #0690	Dako Germany, Hamburg, Germany
Dako Cytomation Pen #S2002	Dako Germany, Hamburg, Germany
Donkey serum	Sigma-Aldrich, Saint Louis, MO, USA
Cryomatrix	Thermo Fisher Scientific, Waltham, MA, USA
Entellan® mounting medium	Merck, Darmstadt, Germany
Mounting medium for fluorescence microscopy	Ibidi, Martinsried, Germany

2.3 Buffer Formulations

Table-3. Buffer Formulations

Buffer	**Containing**
Washing buffer (TBS)	100 mM Tris 150 mM NaCl, pH 7.4 in ddH2O
Citrate Buffer	1.8 mM Citric acid 8.2 mM tri-Natriumcitrat-Dihydrate in ddH2O Adjust pH with NaOH to 6.0
Fixation reagent	4 % Paraformaldehyde in 0.1M PBS
30 % Sucrose	Sucrose (300 g/l) in 0.05 M phosphate buffer
Cryo-protectant buffer	25% Ethylene glycol 25% Glycerol, 50% 0.1M PBS, adjusted to pH 7.4
Antibody diluent buffer	1X PBS 0.3% Triton 5% Donkey serum

2.4 Primary antibodies

Table-4. Primary antibodies

Primary Antibody	Dilution	Company	Catalogue
Rat anti- CD31	1:50	Becton Dickinson	550274
Rabbit anti- Von Willebrand Factor (vWF)	1:400	Dako	A0082
Goat anti- PDGFR-β	1:50	R&D Systems	AF1042
Rabbit anti- Desmin	1:200	Abcam	ab15200
Rabbit anti- CD 248	1:200	Thermo Fischer Scientific	PA5-20436
Rabbit anti- RFP	1:200	Abcam	ab62341
Chicken anti- GFP	1:500	Aves	GFP-1020
Rabbit anti- Ki67	1:400	Abcam	ab16667
Rabbit anti- CD146	1:1000	Abcam	ab75769
Rat anti- CD105	1:200	R&D Systems	AF6440
Rat anti- Sca1	1:100	R&D Systems	MAB1226
Rat anti- CD29	1:200	R&D Systems	MAB2405
Mouse anti- Polysialic- Acid- NCAM [66]	1:100	Millipore	MAB 5324
Mouse anti- CNpase	1:100	Abcam	ab 6319
Mouse anti- S100 (ß Subunit)	1:100	Sigma	S2532
Mouse anti- Tubulin ß III	1:100	Sigma	T8578
Rabbit anti- Iba1	1:500	Wako Pure	019-19741
Goat anti- Iba1	1:500	Abcam	ab5076
Rabbit anti- PU1/spi1_9G7	1:200	Invitrogen	A 13971
Rabbit anti- PU1(9G7)	1:100	Cell Signaling	2258s
Rabbit anti- Sox 2	1:200	Abcam	ab97959
Goat anti- Sox 2	1:400	Novos	AF2018
Rabbit anti- CD45	1:400	Abcam	ab10558
Rabbit anti- CD11b	1:400	Abcam	ab52478
Rat anti- F4/80 (BM8)	1:200	Santa Cruz	Sc-52664
Mouse anti- IDH1-R132H	1:20	Dianova	DIA-H09
Rabbit anti laminin	1:500	Sigma	L9393

2.5 Secondary antibodies

Table-5. Secondary antibodies

Secondary Antibody	Conjugation /Biotinylation	Dilution	Company	Catalogue number
donkey anti- rabbit IgG	Biotinylated	1:250	Jackson Immuno Research	711-065-152

donkey anti-rabbit lgG	Alexa Fluor 488	1:500	Jackson Immuno Research	711-545-152
donkey anti-rabbit lgG	Alexa Fluor 594	1:500	Jackson Immuno Research	711-585-152
donkey anti-rabbit lgG	Alexa Fluor 647	1:500	Jackson Immuno Research	711-606-152
horse anti- goat lgG	Biotinylated	1:250	Vector Labs	BA-9500
donkey anti- goat lgG	Biotinylated	1:250	Jackson Immuno Research	705-065-147
donkey anti- goat lgG	Alexa Fluor 488	1:500	Jackson Immuno Research	705-545-147
donkey anti- goat lgG	Alexa Fluor 647	1:500	Jackson Immuno Research	705-605-003
donkey anti- rat lgG	Biotinylated	1:250	Jackson Immuno Research	712-055-153
goat anti- rat lgG	Biotinylated	1:250	Vector Labs	BA 9400
donkey anti-rat lgG	Cy 5 conjugated	1:500	Jackson Immuno Research	712-175-150
donkey anti- rat lgG	Alexa Fluor 594	1:500	Jackson Immuno Research	712-585-150
donkey anti- rat lgG	Alexa Fluor 647	1:500	Jackson Immuno Research	712-605-153
donkey anti-rat lgG	Cy 2 conjugated	1:500	Jackson Immuno Research	712-225-150
donkey anti-chicken lgG	Biotinylated	1:500	Jackson Immuno Research	703-065-155
donkey anti-chicken lgG	FITC conjugated	1:500	Jackson Immuno Research	703-095-155

2.6 Other reagents for immunostaining

Table-6. Other reagents for immunostaining

Reagents	**Dilution/ Concentration**	**Company**	**Catalogue number**
Alexa Fluor 488-streptavidin conjugate	1:500	Jackson Immuno Research	016-540-084
Alexa Fluor 594-streptavidin conjugate	1:500	Jackson Immuno Research	016-580-084
Alexa Fluor 647-streptavidin conjugate	1:500	Jackson Immuno Research	016-600-084
Biotinylated Isolectin B4 (IB4)	1:400	Santa Cruz	sc1205
TSA Reagent, Biotin-XX Tyramide	1:200	Fisher Scientific	T20947
Dapi4′,6-Diamidin-2-phenylindole (DAPI)	2 µg/ml	Sigma	D 9564

2.7 Commercial kits for immunostaining

Table-7. Commercial kits for immunostaining

Kit	**Provider**	**Country**

MaxFluor™ Mouse on Mouse Fluorescence Detection Kit (MaxFluor 488)	Dianova	Hamburg, Germany
Vectastain Elite ABC Kit (peroxidase standard) PK-6100	Vector	Burlingame, CA, USA

2.8 Human GBM specimens and tumor-free brain tissue

All human specimens were obtained from the tissue bank of Neurosurgical Research Laboratory, University Clinics Munich, LMU. All human GBM were diagnosed with WHO grade IV by neuropathologists. For IDH1-R132H IHC staining, all GBM specimens were detected as IDH1-R132H mutant. Brain tissue from epilepsy patients was set as the tumor-free control in all experiments. Ethical approval was given as *Project 18-304*.

2.9 Glioma cell lines

Table-8. Glioma cell lines

Glioma Cell line	**subtypes**
Murine glioma GL261 cells	
Murine transgenic glioma cells (CDKN2a$^{-/-}$-EGFRvIII-GFP NPCs)	classical
Murine transgenic glioma cells (TP53$^{-/-}$-PDGFB-GFP NPCs)	proneural
Human glioma cells GBM#2	classical
Human glioma cells GBM#14	non-classified
Human glioma cells NCH644	proneural

2.10 Cell culture medium and reagents

Table-9. Cell culture medium and reagents

Medium/ reagent	**Catalogue number**	**Company**
Dulbecco's MEM (DMEM)	Biochrom GmbH, Berlin, Germany	FG0415
DMEM/F12 Medium	Gibco, NewYork, USA	11320-74
Neuocult™ Basal Medium (mouse)	STEMCELL Technologies, Vancouver, Canada	05700
Fetal Bovine Serum (FBS)	Biochrom GmbH, Berlin, Germany	S0615
B-27 supplement(50X)	Gibco, NewYork, USA	17504-044
MEM Non-Essential Amino Acids Solution (100X)	Life Technologies, New York, USA	11140-050
Neuocult™ Proliferation Supplement(mouse)	STEMCELL Technologies, Vancouver, Canada	05701
Penicillin-Streptomycin (P/S)	Life Technologies, Bleiswijk Netherlands	10378-016

hFGF	PeproTech GmbH, Hamburg, Germany	100-18B
hEGF	PeproTech GmbH, Hamburg, Germany	AF-100-15
StemPro Accutase Cell Dissociation Reagent	Gibco, NewYork, USA	A11105-01
Trypsin/EDTA solution(10X)	Biochrom GmbH, Berlin, Germany	L2153
Trypan Blue solution	Sigma, UK	T8154
Aqua (sterilized)	B.Braun Melsungen AG, Melsungen, Germany	6724092.00.00
PBS (sterilized)	Apotheke Klinikum der Universität München, Munich, Germany	L20170802-03

2.11 Mouse strains

Table-10. Mouse strains

Mouse Strains	Referred to
Nestin_CreER^{T2}, Ai9-tdTomato mice	Nestin-reporter mice
Nestin_CreER^{T2}, R26_LSL_diphtheria toxin subunit alpha (DTA), Ai 9 mice	IDTA mice
Nestin_CreER^{T2}, SOX2$^{fl/fl}$, Ai9-tdTomato mice	SOX2-cKO mice
Pu.1^{GFP} mice	
Pu.1^{GFP}, Nestin_CreER^{T2}, Ai9-tdTomato mice	Pu.1^{GFP}; nestin-reporter mice
Nestin_CreER^{T2}, CCR2 $^{GFP/+}$, Ai9-tdTomato mice	CCR2$^{GFP/+}$; nestin-reporter mice
Nestin_CreER^{T2}, CX3CR1$^{GFP/+}$, Ai9-tdTomato mice	CX3CR1$^{GFP/+}$; nestin-reporter mice
FMS-like tyrosine kinase-3 (Flt3)_cre, Rosa$^{mT/mG}$ mice	Flt3_cre; Rosa$^{mT/mG}$ mice
C57BL/6 mice	
Athymic nude mice	

2.12 Drugs for animal experiments

Table-11. Drugs for animal experiments

Drug	Company
Bepanthen® Eye- and Nose- cream	Bayer HealthCare, Leverkusen, Germany
Ketaminhydrochlorid (Ketavet, 100 mg/ml)	Pfizer, New York City, NY, USA
Rompun (2%) & Xylazine	Bayer Vital GmbH, Leverkusen, Germany
Tamoxifen (T5648)	Sigma-Aldrich, Saint Louis, MO, USA
Corn Oil (C8267)	Sigma-Aldrich, Saint Louis, MO, USA
0.9% NaCl (sterilized)	B.BRAUN Melsungen AG, Melsungen, Germany

2.13 Computer Software

Table-12. Computer Software

Software	Company
Leica LAS X Core offline version 1.9	Leica Microsystems Vertrieb GmbH, Wetzlar, Germany
Leica Microsystems LAS SP8	Leica Microsystems Vertrieb GmbH, Wetzlar, Germany
Stereo Investigator	MBF Bioscience, Williston, Vermont, USA
Image J	NIH, Bethesda, MD, USA
GraphPad PRISM 7	Graph Pad Software Inc., La Jolla, CA, USA
Adobe Photoshop CC 2017	Adobe Systems Inc., San Jose, CA, USA
Adobe Acrobat XI Pro	Adobe Systems Inc., San Jose, CA, USA
Microsoft Office 2016	Microsoft, Redmond, WA, USA
Thomson Reuters EndNote X 8.2	Thomson Reuters, Philadelphia, PA, USA

3. Methods

3.1 Cell culture

Murine GBM cells Gl261 were cultured with 10% FCS/ DMEM medium (with 1x MEM-NEAA and 1% Penicillin-streptomycin). Human GBM cells (GBM14, NCH644) and transgenic murine glioma cells (CDKN2a$^{-/-}$-EGFRvIII-GFP, P53$^{-/-}$-PDGFB-GFP) were cultured as spheres with F12/ DMEM medium (with 1x B-27 supplement, 1% Penicillin-streptomycin, 10ng/ml hFGP and 10ng/ml hEGF). Human GBM cells GBM2 were cultured as spheres with Neurocult^{TM} Basal Medium (with 10% Neurocult^{TM} Proliferation Supplement, 1% Penicillin-streptomycin, 10ng/ml hFGP and 10ng/ml hEGF). Cells were split into single cells and diluted into 100,000 cell/µl (Gl261) or 50,000 cell/µl (all other cell lines) with 1x PBS for tumor inoculation.

3.2 Animal experiment models

3.2.1 Cre/loxP system

Several transgenic mouse strains were used for this study (Table-10). Some of them carried the Cre (cyclization recombination) /loxP (locus of crossing [x-ing]-over of bacteriophage P1) system. The Cre/loxP is a commonly used tool for manipulating conditional somatic mouse mutants[67]. In Cre/loxP system, the site-specific DNA recombinase Cre can excise the selected intervening DNA sequence of two 34-bp DNA recognition sites named loxP[67,68]; the estrogen receptor ligand-dependent chimeric Cre recombinases (CreER) can be activated by the estrogen receptor ligand, 4-hydroxytamoxifen, which is a metabolite of tamoxifen[67,69].

3.2.2 Nestin::CreER^{T2}:: R26-RFP mice

Nestin (Nes) is an intermediate cytoskeletal filament initially described in neural stem cells[70]. Nestin contributes to the proliferation and differentiation of stem cells[70,71]. Nestin:: CreER^{T2} mice express a CreER fusion protein under the control of a nestin promoter. R26-RFP (Ai9) mice carry a Cre reporter allele which harbours a loxP-flanked (flox) STOP cassette preventing transcription of a CAG promoter-driven red fluorescent protein (RFP) variant (Ai9-tdTomato)[72]. As showed in the schematic diagram below, Nestin:: CreER^{T2}, R26-RFP mice (Nestin-reporter) are generated by crossbreeding Nestin::CreER^{T2} mice with Ai9-tdTomato mice. After tamoxifen administration, CreER is induced to enter into the nucleus and recombine loxP sites to

remove the floxed sequence. Cre recombinase-expressing cells and their daughter cells are induced to express RFP and can be detected with a fluorescence microscope.

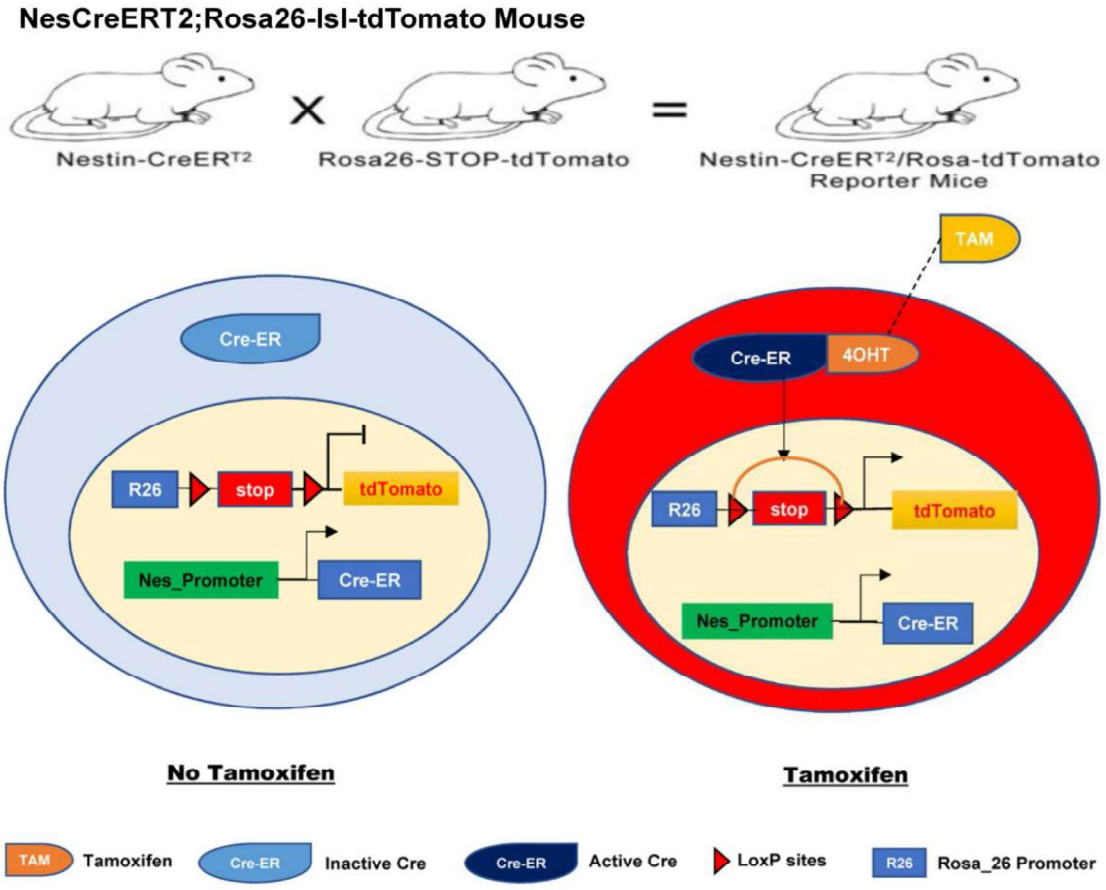

Figure-3. The mechanism of RFP expression in traced cells in nestin-reporter models. Nestin-reporter mice were generated by crossbreeding Nestin::CreER2 mice and R26-RFP mice. In target cells, the Cre recombinase is activated by tamoxifen administration. The Cre recombinase cuts out the floxed STOP sequence[68]. These cells and their daughter cells are therefore labelled with RFP[67].

3.2.3 other transgenic mouse models

The transcription factor Sox2(Sex-determining region Y-box2 protein) is a key regulator in CNS stem cell. In the Nestin::CreER^{T2}, SOX2$^{fl/fl}$, R26-RFP mice (SOX2 conditional knock out, Sox2-cKO), SOX2 can be knocked out in traced cells[73]. The IDTA Nestin- reporter mouse is a transgenic mouse line for the ablation of Cre-induced cells due to the Cre-induced expression of diphtheria toxin A (DTA)[74].

CX3CR1 is expressed in myeloid cells, not only in macrophages but also in microglia[75]. CX3CR1$^{GFP/+}$ Nestin-reporter double-transgenic mice are applied for the identification of myeloid cells.

CCR2 is expressed in monocytes and macrophages[55], but not in microglia[75].Using CCR2 $^{GFP/+}$; nestin-reporter double-transgenic mice, we can distinguish whether RFP expressing cells are monocyte-derived macrophages.

The transcription factor PU.1 is a key regulator during the development of lymphoid and myeloid cells[76-79], including microglia[77,78]. The Pu.1^{GFP} mouse is a green fluorescent protein reporter mouse line, and it is a good tool to visualize microglia and macrophages inside and outside of the CNS.

FMS-like tyrosine kinase 3 (Flt3) is expressed in fully multipotent mouse hematopoietic progenitor cells and plays essential roles in the earliest stage of normal development of normal granulocyte-monocyte progenitor[80]. The Flt3_cre; Rosa$^{mT/mG}$ mouse is a Cre-induced GFP reporter mouse line to monitor bone marrow derived myeloid cells.

3.2.4 Other animal experimental models

Bone marrow [66] chimeric mice[82] were built up by Roland Kälin after lethal irradiation (split dose of 600 rad at day1). After irradiation, wild-type mice (C57BL/6J) mice were intravenously injected with 5 x 10^6 BM cells from donors (nestin-reporter mice). For the control group, nestin-reporter mice were radiated and then transplanted with 5 x 10^6 BM cells from Pu.1-GFP mice. After two months, they were orthotopically inoculated with Gl261 cells. Tumors were harvested 14days post-operation (DPO) for further investigation.

Additionally, we produced xenograft orthotopic human GBM models with athymic nude mice. Some wildtype mice (C57BL/6J) were also used in this study to generate different subtypes of murine GBM.

3.3 Animal experiments

3.3.1 Laboratory animal maintenance

All our animal experiments were approved by the government agency of Upper Bavaria, and all our operations and management strictly follow the German Animal Protection Act Guidelines. All *in vivo* experiments were performed in the Walter Brendel Centre for Experimental Medicine, LMU Munich. Animals were kept in a standardized animal house with enough water and food, and they were inspected every day after the operation.

3.3.2 Experimental schemes

In this study, animals were sub-grouped into 7/14/21 DPO groups (Fig. 4). On day 0, mice were orthotopically implanted with GBM cells. Then, all mice received intraperitoneal (i.p.) tamoxifen injections three times post operation. Mice were sacrificed at the end of the schedule.

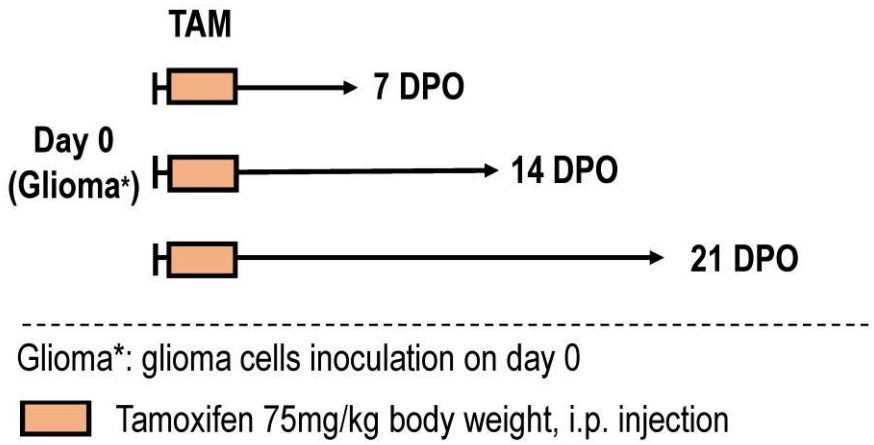

Figure-4. Animal experimental schemes. All mice were inoculated with glioma cells on day 0 and injected with tamoxifen. For 7 DPO groups, tamoxifen was i.p. injected on day 1, 2 and 3; for 14 and 21 DPO groups, tamoxifen was i.p. injected on day 1, 2 and 3. The dose of tamoxifen for each injection was 75 mg /kg body weight.

3.3.3 Orthotopic glioma inoculation

Orthotopic glioma implantation mouse models were produced to investigate the tumor environment and tumor angiogenesis *in vivo*. Inoculation procedures were as follows[18]: Firstly, mice were i.p. injected with the animal anaesthetic drug (a mixture of 0.36 ml 2% Rompun, 1.02 ml 10% ketamine, and 4.86 ml 0.9% NaCl), with a dosage of 7µl drug-solution per gram of mouse weight. Their corneas were protected with Bepanthen® eye and nose ointment. Secondly, the head was placed onto a stereotactic frame and fixed in the flat-skull position. A midline incision was cut on its head after disinfection with 10% potassium iodide solution. The injection point was located at 1.5 mm anterior and 1.5 mm right of the bregma (Fig. 5). A hole was made by drilling with a 23-gauge needle tip. A syringe was inserted 4 mm into the mouse brain vertically. A small space was made in the mouse brain after moving the syringe 1mm up. Then, 1µl glioma cell suspension (with 10^5 Gl261 cells or $5*10^4$ other glioma cells) was injected into the mouse brain at 0.5µl per minute. After the inoculation, the needle was removed carefully and slowly at 1mm per minute. Finally, the wound was sewed, and the animal was returned to the animal facility.

Figure-5. Orthotopic glioma inoculation. A mouse is placed and fixed on a stereotactic frame.

3.3.4 Perfusion and tissue preparation

Perfusion was conducted at the end of the experiment schedule. A mouse was first anaesthetized and fixed on an operating platform. Then, a thoracotomy was performed to expose the heart. An extra circulation was built up with a cut on its atrium and a transfusion needle into the left ventricle of the heart, and an extracorporeal pump system drove this extra circulation with speed at 8.7 ml/min. 10 ml ice-cold sterilized PBS was pumped to wash out its blood. Then 10 ml fixation reagent was injected to fix its brain. Another 5 ml PBS was applied to wash the fixation reagent. After the perfusion, the mouse brain was carefully collected and fixed in the fixation reagent for 24 hours at 4°C. Mouse meninges were dissected under microscope with the method described by Antoine Louveau and Jonathan Kipnis[83].

The brain tissue was soaked in 30% sucrose until the tissue was dehydrated and sank to the bottom of the container. Afterwards, it was embedded with Cryo-matrix in a light-protected box, and frozen above liquid nitrogen. The brain was cut into 40μm horizontal sections and preserved as free-floating sections in a 24-well-plate filled with cryo-protectant buffer. All tissue was stored at −20°C and protected from light.

3.3.5 Cell isolation from mouse meninges and co-transplantation

The transplantation experiment was designed for the exploration of whether the RFP+ cells were derived from meninges. Cells were isolated from mouse meninges and then transplanted into nude mice brains together with GBM cells. Procedures were as follows:

a) Kill the mouse, disinfect the whole body with 95% ethanol, and wait for 10 minutes.
b) Cut the neck of the mouse and discard its body.
c) Remove the mouse skin and muscle of the head.
d) Cut off the skull base and the nasal bone.
e) Wash away the brain tissue from the scalp with sterilized PBS in a 50ml Falcon tube three times, left the meninges attached to the scalp.
f) Remove all soft tissue except meninges on the surface of the scalp with microsurgical forceps.
g) Wash in 6-wells plates with sterilized PBS for three times.
h) Digest the meninges with 2ml Trypsin in 37°C incubator for 20 minutes.
i) Stop the digestion with 6ml 10% FCS medium, centrifuge it at 800 rpm for 5 minutes.
j) Discard the supernatant and add 200µl sterilized PBS. Count the cell numbers.
k) Mixed the meninges cells with 500,000 Gl261 cells, and centrifuge with 1000 rpm for 5 minutes.
l) Re-suspend them with 5µl sterilized PBS, inoculated them into nude mice with the method as described above.

3.4 Histology and immunohistochemistry

3.4.1 HE staining

Hematoxylin-eosin staining (HE staining) is the most common staining technique in histology[84]. This staining was conducted in order to check if there was a tumor or to estimate the individual tumor volume. Procedures were as follows:

a) Mounting the sections
b) Dehydration in 100% Ethanol for 30 seconds.
c) Stain in Meyer's Hemalaun solution for 2 minutes.
d) Rinse in running tap water for 5 minutes.
e) Counterstain with 0.5% Eosin G-solution for 30 seconds.

f) Dip shortly in water.
g) Dehydration through ascending concentration of alcohol series starting with 70% EtOH for 30 seconds.
h) Continue by 96% EtOH for 1 minute.
i) Continue by 100% EtOH for 1 minute.
j) Continue by Roti®-Histol for 1 minute.
k) Repetition of the last step with fresh Roti®-Histol.
l) Cover with mounting medium.

3.4.2 Immunohistochemistry

In this study, immunohistochemistry (IHC) was conducted to identify the specific molecular markers of the target cells. For all IHC staining, a negative control was always set to exclude unspecific reactions. A positive control was applied for comparing the experimental outcome. General procedures were as follows:

a) Wash with washing buffer (Table. 3) 3 x 5 minutes at room temperature.
b) Block the nonspecific sites with PBS, 0.3% Triton X-100, 5% donkey serum for 30 minutes at room temperature.
c) Dilute the primary antibody with the antibody diluent buffer (Table. 3). Incubate the tissue with primary antibody overnight at 4 °C.
d) Wash with washing buffer 3 x 5 minutes at room temperature.
e) Incubate with secondary antibody for two hours at room temperature.
f) Wash with washing buffer 3 x 5 minutes at room temperature.
g) Incubate with Dapi (1:10,000) for 2 min at room temperature as a nuclear stain. Wash with wash buffer 3 x 5minutes at room temperature.
h) Mount brain sections on a glass slide. Put it in the dark and wait until it is dry.
i) Cover with the fluorescence mounting medium.

In some cases, the Labeled Streptavidin-Biotin (LSAB) method, which the fluorescent-dye labelled streptavidin could specifically bind with the biotinylated antibody, was used as a candidate when the specific fluorescein was not available.

Some other specific IHC methods were also used in this study. Protocols are described as follows:

IHC Staining with Mouse-on-mouse kit

With a Dianova MaxFluor™ Mouse on Mouse Fluorescence Detection Kit, mouse antibodies could also be used to detect some specific antigens on murine specimens,

such as Cnpase, NeuN, S-100β, Tubulin ß III, and Polysialic-Acid-NCAM. Procedures are as follows:

a) Wash with PBST (PBS, 0.1% Tween-20) 3 x 5 minutes at room temperature
b) Mount and circling the sections with a Dako Cytomation Pen.
c) Rinse with PBST 3 x 2 minutes at room temperature
d) Block with Protein blocking solution (reagent 1) for 10 minutes at room temperature.
e) Block with mouse IgG with M.O.M.^{TM} mouse IgG Blocking Reagent (reagent 2) for one hour at room temperature.
f) Rinse with PBST 3 x 2 minutes at room temperature.
g) Incubate with primary antibody overnight at 4 °C. Primary antibody was diluted in Dako antibody diluent Dako S3002.
h) Wash with PBST 3 x 2 minutes at room temperature.
i) Incubate with Fluorescence signal enhancer (reagent 3) for 30 minutes at room temperature
j) Wash with PBST 3 x 2 minutes at room temperature.
k) Incubate with Max Fluor labelled linker (reagent 4) 1:200 diluted in Fluorescent Diluent (reagent 5) for two hours at room temperature.
l) Wash in PBST 3 x 2 minutes at room temperature.
m) Incubate with Dapi (1:10,000) for 2 minutes at room temperature as a nuclear stain.
n) Rinse with PBST 3 x 2 minutes at room temperature.
o) Cover with the fluorescence mounting medium.

IHC Staining for paraffin-embedded tissue

The protocol of IHC staining on paraffin-embedded human tissue is as follows:

a) Deparaffin the tissue sections in 60 °C isopropanol for 2 x 20 minutes.
b) Fixation in 70% -20°C Aceton for 10 minutes.
c) Wash with wash buffer 3 x 5 minutes.
d) Circle the sections with a Dako Cytomation Pen.
e) Cooked with Citrate Buffer (Table.3) at 100 °C for 20 minutes.
f) Cool down to room temperature in 20 minutes.
g) Wash with the wash buffer 3 x 5 minutes.
h) Block the endogenous peroxidase with Dako endogenous enzyme block (Dako S2003) for 10 minutes at room temperature.

i) Wash with washing buffer 3 x 5 minutes.
j) Block with Protein Blocking Reagent (Dako X0909) for one hour at room temperature.
k) Tilt the slide to remove the protein block reagent.
l) Primary antibody diluted in Dako antibody diluent (Dako S3002). Incubate overnight at 4 °C.
m) Wash with washing buffer 3 x 5 minutes.
n) Fluorophore coupled Streptavidin diluted in Dako antibody diluent (Dako S3002) for two hours at room temperature.
o) Wash with washing buffer 3 x 5 minutes.
p) Incubate with Dapi (1:10,000) for 2 minutes at room temperature as a nuclear stain.
q) Mount and cover with fluorescence mounting medium.

3.5 Microscopy

The evaluation of HE staining was performed with a Zeiss Axioskop-2 light microscope. Fluorescence quantification analysis was conducted with an Axio Observer A1 inverse fluorescence microscope and a Zeiss Axiophot fluorescence microscope.
All confocal images were acquired with a Leica confocal laser microscope SP8 Upright Confocal 405/WLL Phys Stand. A 40x objective lens and a 63x objective lens were used to take confocal pictures or 3D images in this study. The format for all images was 1024 x 1024 pixels. The settings of the laser power and the gate referred to the positive and negative controls. Sequentially Z-stack were conducted for all confocal images. The Zoom-In factor was set as 2 to 5 times in some cases. The Tile- Scan was applied for searching the interesting cells and the quantification of RFP cells in 7 DPO groups[85]. Confocal images stacks were processed with the ImageJ software and LAS Montage Imaging software (Leica).

3.6 Cell number quantification

All mouse brains were generally inspected for their tissue quality, tumor volume, the distribution and the morphology of RFP+ cells. Mouse brains with good tissue quality were selected for further analysis. The quantification included total RFP+ cell numbers, vascular RFP+ cell numbers, avascular RFP+ cell numbers, Sox2+ /RFP+ cell numbers and CD11b+/RFP+ cell numbers. Generally, cell numbers were counted under a 20X

objective lens with a fluorescence microscope. For each mouse, at least 15 fields were selected for counting. Cells were counted according to their nucleus on DAPI staining. Sox2+/RFP+ cell numbers and CD11b+/RFP+ cell numbers were evaluated after IHC staining. The 40X and 100X objective lens was applied to distinguish whether the cell is positive for double/triple markers.

For 7 DPO tumors, cell numbers were analyzed with a confocal microscope. Fields were randomly selected with the tile-scan program[85]. Numbers of target cells with or without the specific marker were evaluated according to the manufacturer's protocol.

3.7 Tumor size quantification

For tumor volume evaluation, every 12th axial section with GBM was inspected under the BMS D1-223A light microscope after H-E staining[18]. Tumor volume was quantified according to the Cavalieri principle by analyzing the tumor area in every brain section. Stereoscopic coordinates of brain slices with GBM were used to calculate the tumor infiltration in the vertical axis. A tumor volume per mouse was obtained by multiplying this vertical-axis with the average brain tumor area per brain section.

3.8 Vascular analysis with Stereo-investigator

Vascular stereological analysis was performed for the tumor area of vWF-positive green fluorescent vessels on every 12th section. It was conducted with the Stereo-Investigator 10.21.1 (Micro-Bright-Field Bioscience) connect to an Olympus-BX53-microscope (Olympus Europe), which was equipped with a motorised stage (Micro-Bright-Field Bioscience)[18]. More than 100 sampling sites per mouse were inputted into the Stereo-investigator, and they read out with branch points, vessel length and vessel length-density.

3.9 Statistical analysis

GraphPad PRISM 7 software was used for experimental statistical analysis. For all experimental groups, an unpaired, non-parametric student's t-test was applied to compare two samples. Multiple samples were evaluated by one-way ANOVA together with a Newman-Keuls post-hoc test. Also, a Kaplan-Meier survival curve with the Log-rank (Mantel-Cox) test was made for animal survival experiments. Bar-diagrams showed a mean-values ± standard deviation of the mean; statistical significance was assumed if $P<0.05$; P-values were present in figures as *, $p<0.05$; **, $p<0.01$; ***, $p<0.001$; ****, $p<0.0001$; N.S., no significance.

4. Results

4.1 Vascular and avascular RFP expressing cells in the GBM microenvironment of nestin-reporter models

RFP expressing cells were inspected at 7, 14 and 21 DPO GBM in nestin-reporter mice (Fig. 6A). According to the location of RFP expressing cells, they were classified into vascular cells and avascular cells (Fig. 6B). Vascular and avascular cells numbers in 7, 14 and 21 DPO tumors were quantified (Fig. 6C-E): vascular RFP expressing cell numbers were 9.56 ± 1.17 (n=6) at 7 DPO, 13.67 ± 3.255 (n=4) at 14 DPO, and 27.10 ± 5.643 (n=5) at 21 DPO (Fig. 6C-D). Comparing to 7 DPO, vascular RFP expressing cell numbers of 21 DPO tumors increased ($p=0.009$). Avascular RFP expressing cell numbers were 10.3 ± 0.78 (n=6) at 7 DPO, 10.91 ± 3.14 (n=4) at 14 DPO, and 2.68 ± 0.49 (n=5) at 21 DPO: avascular RFP expressing cells appeared in GBM in the early phase of tumorigenesis, while they diminished later (Fig. 6E).

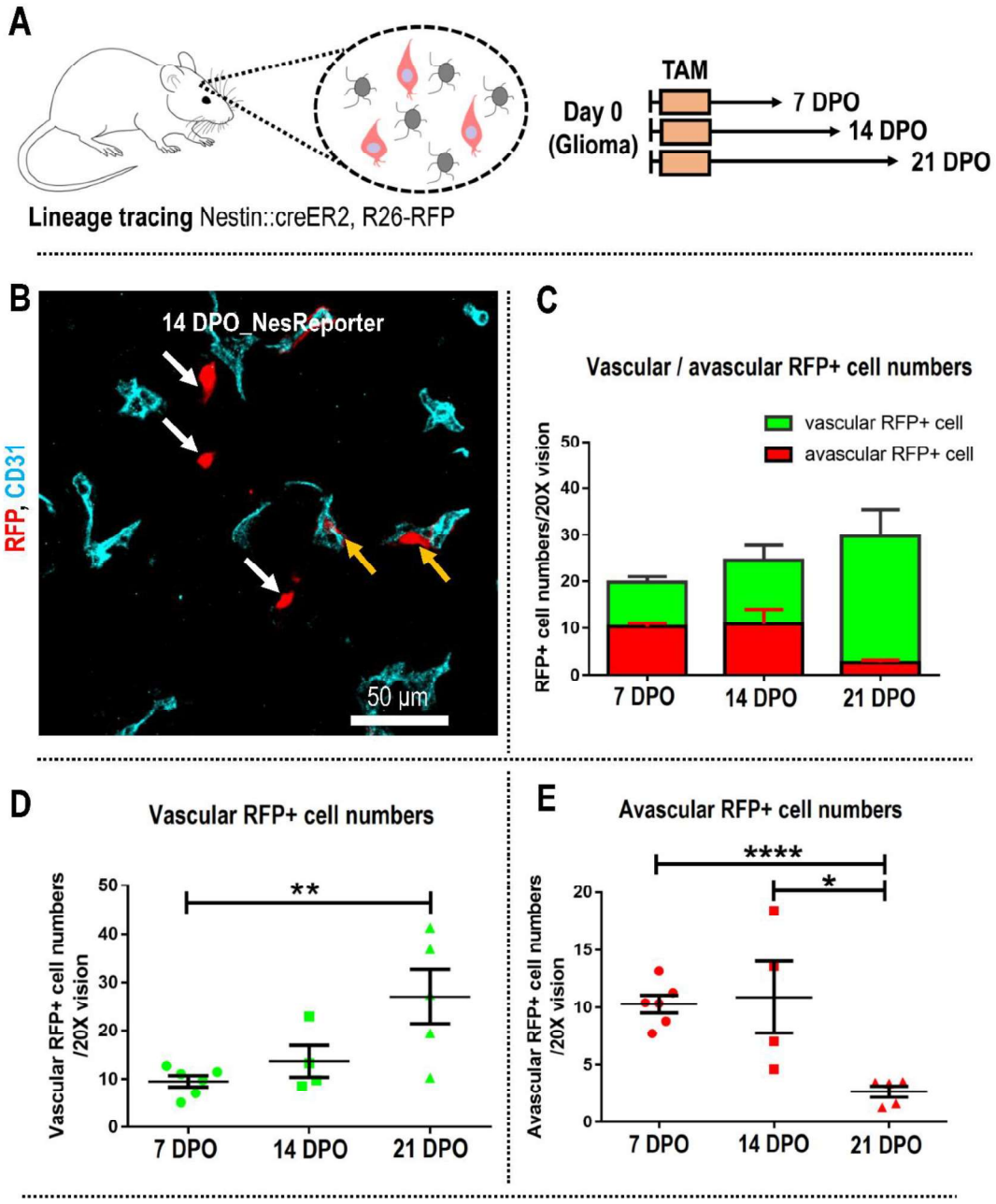

Figure-6. Vascular and avascular RFP expressing cells in the GBM microenvironment of nestin-reporter models. **(A)** nestin-reporter mice were sub-grouped into 7DPO, 14DPO and 21DPO groups, and they were inoculated with Gl261 on day 0. They were injected with tamoxifen for 3 connective days after tumor injection. **(B)** Using immunofluorescence staining for endothelial cells marker CD31 on 14 DPO tumors, RFP expressing cells were classified into vascular (yellow arrows) and avascular cells (white arrows). Scale bar, 50μm. **(C)** Vascular and avascular RFP expressing cell numbers in every 20x field of 7 DPO, 14 DPO or 21 DPO tumors. **(D)** The analysis of vascular RFP expressing cell numbers of 7 DPO, 14 DPO or 21 DPO tumors. Vascular RFP expressing cell numbers increased during the tumorigenesis. **(E)** The analysis of avascular RFP expressing cell numbers of 7 DPO, 14 DPO or 21 DPO tumors. Avascular RFP expressing cells were found in GBM in the early phase of tumorigenesis, while they diminished later.

4.2 Vascular RFP expressing cells are pericytes

Using IHC staining for pericyte markers and endothelial cell markers on 14 DPO tumors (Fig. 7A-B), large numbers of vascular RFP expressing cells were found to express desmin or PDGFR-β: these vascular RFP expressing cells were identified as pericytes. We also found that all PDGFR-β/RFP double-expressing cells were perivascular cells (Fig. 7C-D). Vascular RFP expressing cells shared other pericyte markers (Table-13), such as NG2, CD248, and CD146. However avascular RFP expressing cells were PDGFR-β negative (Fig. 7D).

No RFP expressing pericytes expressed the myeloid marker CD11b (Fig. 7E), and RFP expressing cells were always CCR2 negative (Fig. 7F). Except for pericyte markers and myeloid markers, some other cell markers were also absent from vascular RFP expressing cells at 7 DPO (Table-13). Among them, MSC markers (CD29 and Sca1) were not detected on these vascular RFP-positive cells (Fig. 7G-H), which indicated that these pericytes did not overlap with MSC.

It was reported that the majority of pericytes in GBM differentiated from glioma stem cells[86]. However, RFP expressing intratumoral pericytes were abundant in the nestin-reporter model at 21 DPO. All these traced cells must be host-derived. On IDH1-R132H mutant human GBM, we performed an IHC-staining for detecting the glioma-inheritating marker IDH1-R132H together with the pericyte-marker PDGFRβ and we never observed pericytes that were derived from glioblastoma stem cells (Fig. 7I).

Table-13. Molecular markers of vascular RFP expressing cells

Markers	**RFP+ vascular cells**
Positive	PDGFRβ, Desmin, NG2, CD248, CD146
Negative	CD11b, CD45, F4/80, Iba1, Sox2, Sca1, CD29, CD105, CD44, NeuN, Tuj1, Cnpase, PSA-NCAM, Doublecortin, MBP, GFAP, S100B

Table-13. Molecular markers of vascular RFP expressing cells. Using IHC staining for pericyte markers (PDGFRB, desmin, NG2, CD248 or CD146), MSC (Sca1, CD29, CD105, CD44), mature and immature neurons (Tuj1, PSA-NCAM, DCX, NeuN), oligodendrocytes (CNPase, MBP) o, astrocytes (GFAP, S100B) or TAM (CD11b, CD45, F4/80, Iba1) on GBM of the nestin-reporter models[58,87-90], we found vascular RFP expressing cells could be labelled with pericyte markers but were absent with other markers (as showed on the table) .

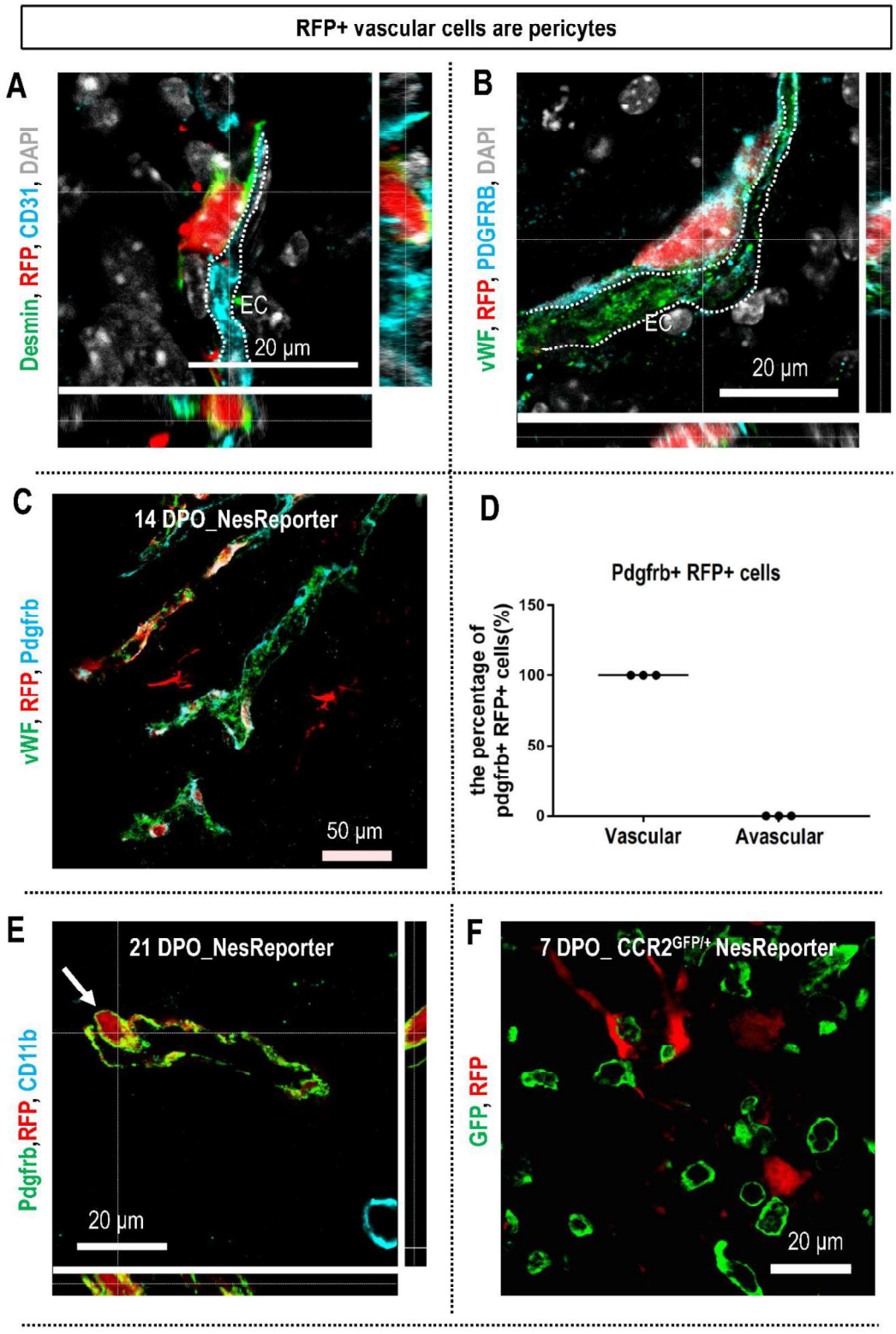

Figure-7. Vascular RFP expressing cells are pericytes. (A-B) Vascular RFP expressing cells shared pericyte markers (Pdgfr-b and desmin). Von Willebrand factor (vWF) is an endothelial cell (EC) marker. Scale bar, 20μm. In 14DPO tumors, avascular RFP expressing cells were Pdgfrb negative and all Pdgfrb/RFP co-expressing cells were vascular cells. Scale bar, 50μm. **(E)** no RFP expressing pericyte showed the myeloid marker CD11b. Scale bar, 20μm. **(F)** In 7DPO tumors of CCR2$^{GFP/+}$; nestin-reporter double-transgenic mice, no RFP expressing cell overlapped with GFP. Scale bar, 20μm.

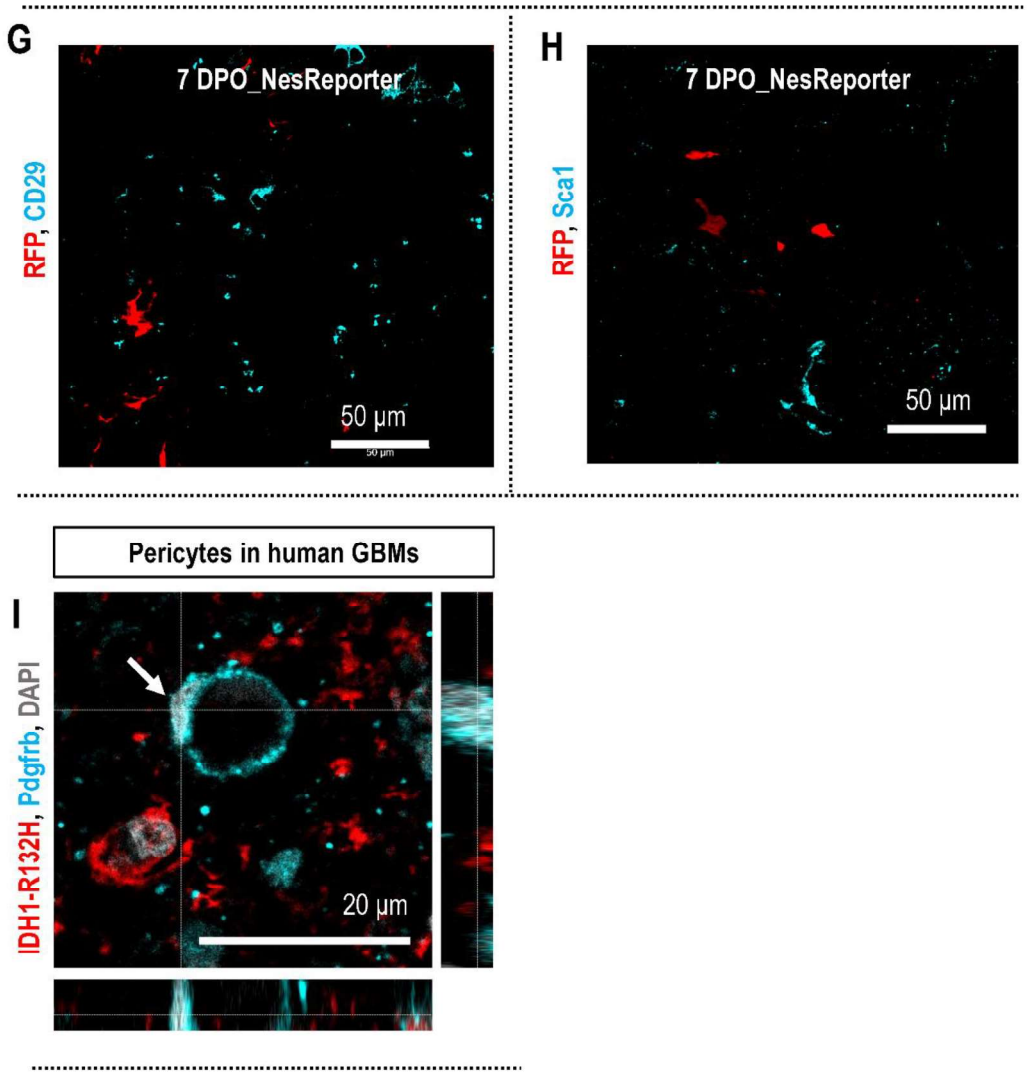

Figure-7. **(G-H)** In 7DPO GBM, no RFP expressing cell expressed mesenchymal stem cell markers, CD29 and Sca1. Scale bar, 50µm. (**I**) In IDH1-R132H-mutated human GBM, many pericytes were detected as IDH1-R132H free. Scale bar, 20µm.

4.3 Avascular RFP expressing cells are tumor-associated cells with a myeloid-like expression profile (TAMEP)

Similar to healthy microglia in Pu.1^{GFP} mice (Fig. 8A), avascular RFP+ cells expressed myeloid cell marker CD11b in a low level (Fig. 8B). Also, avascular RFP+ cells were F4/80 positive, CD45 negative and Iba1negative (Fig. 8C-D). A small number of avascular RFP+ cells expressed myeloid transcriptional factor Pu.1(Fig. 8E).

In 7DPO GBM of Cx3cr1^{GFP}; nestin-reporter double-transgenic mice, some RFP/GFP double-expressing cells were observed (Fig. 8F) and they never expressed Iba1 (Fig. 8G), which indicated that these avascular RFP expressing cells were non-canonical

myeloid cells. Other cell markers were also tested, such as PDGFRβ, desmin, NG2, CD248, CD146, sca1, CD29, CD105, CD44, NeuN, CNPase, PSA and double-cortin, and they were negative on avascular RFP expressing cells (Table-14).

Table-14. Molecular markers of avascular RFP expressing cells

Markers	**Avascular RFP expressing cells**
Positive	CD11b, F4/80, CX3CR1, Pu.1, Sox2
Negative	Iba1, CD45, CCR2, PDGFRβ, desmin, NG2, CD248, CD146, Sca1, CD29, CD105, CD44, Tuj1, NeuN, CNPase, MBP, PSA-NCAM, Doublecortin

Table-14. Molecular markers of avascular RFP expressing cells. Using IHC staining for pericyte markers (PDGFRB, desmin, NG2, CD248 or CD146), mesenchymal stem cells (Sca1, CD29, CD105, CD44), mature and immature neurons (Tuj1, PSA-NCAM, DCX, NeuN), oligodendrocytes (CNPase, MBP) , astrocytes (GFAP, S100B) ,TAM (CD11b, CD45, F4/80, Iba1), myeloid transcriptional factor (Pu.1) or stem cell transcriptional factor (Sox2) on GBM of the nestin-reporter models[58,87-90], we found avascular RFP expressing avascular cells could be labelled with some myeloid markers (CD11b, F4/80), myeloid transcriptional factor (Pu.1) and stem-cell transcriptional factor (Sox2). In 7DPO GBM of $CX3CR1^{GFP}$; nestin-reporter double-transgenic mice, we found avascular RFP expressing cells were labelled with CX3CR1-GFP. While in 7DPO GBM of $CCR2^{GFP}$; nestin-reporter double-transgenic mice, we never found avascular RFP+ cell with macrophage marker CCR2-GFP.

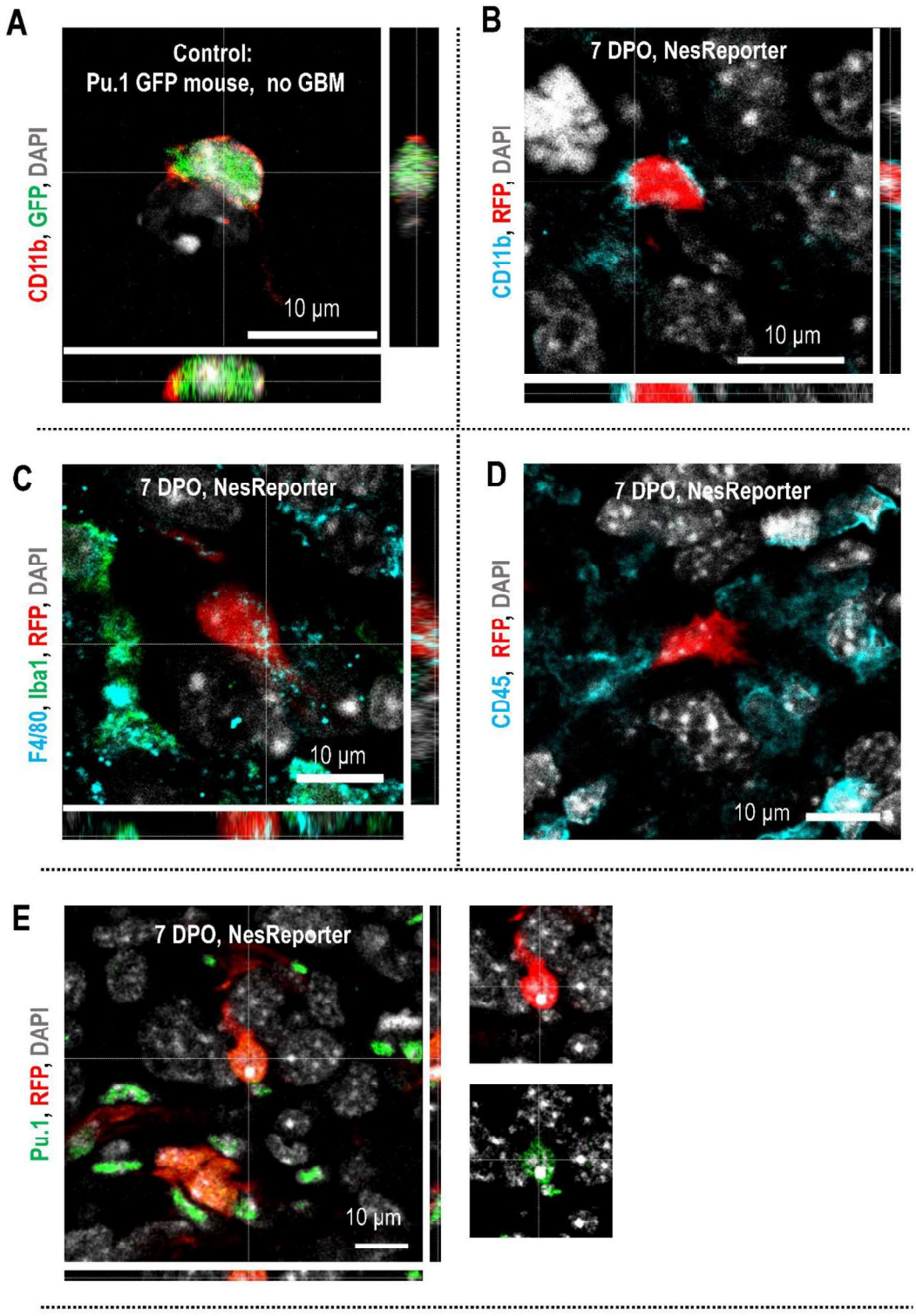

Figure-8. Avascular RFP expressing cells are TAMEP. (A) microglia in healthy Pu.1^{GFP} mice[66] expressed CD11b. **(B)** avascular RFP expressing cells expressed myeloid cell marker CD11b[66]. Avascular RFP expressing cells were F4/80 positive, Iba1 negative and CD45 negative. **(E)** Some avascular RFP expressing cells expressed myeloid transcription factor Pu.1. Scale bars, 10µm.

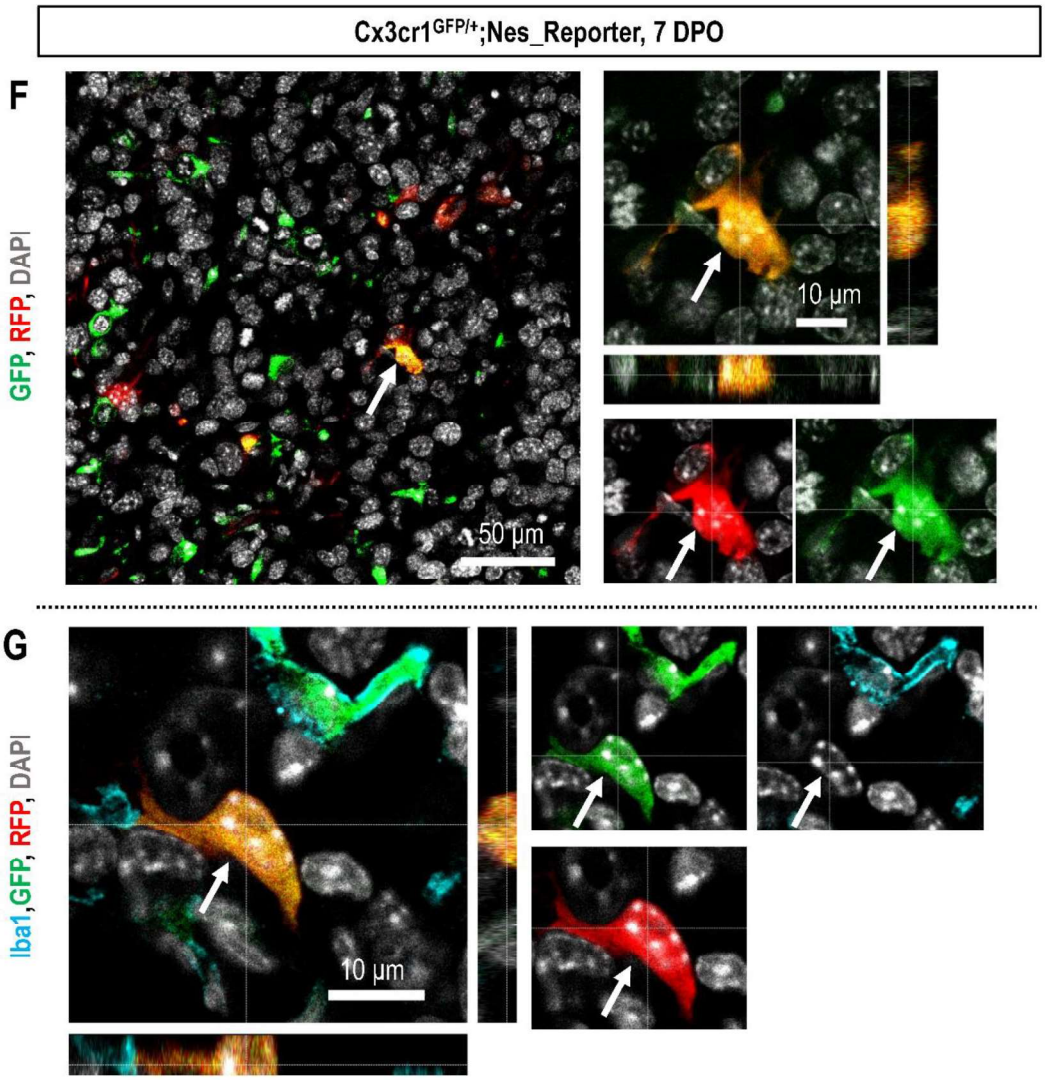

Figure-8. (F) In 7 DPO tumors of Cx3cr1^{GFP}; nestin-reporter double-transgenic mice, some avascular RFP expressing cells overlapped with Cx3cr1-GFP. **(G)** RFP/GFP double-expressing myeloid cells were Iba1 negative in 7 DPO tumors of Cx3cr1^{GFP}; nestin-reporter double-transgenic mice. Scale bar, 10µm.

4.4 Sox2 is expressed in avascular RFP expressing cells, but not in vascular RFP expressing cells

Sox2, a stem cell transcriptional factor[91,92], was expressed in some avascular RFP expressing cells (Fig. 9A-B). All vascular RFP expressing cells were Sox2 negative (Fig. 9C-G) and all Sox2/RFP double-expressing cells were avascular cells (Fig. 9G).

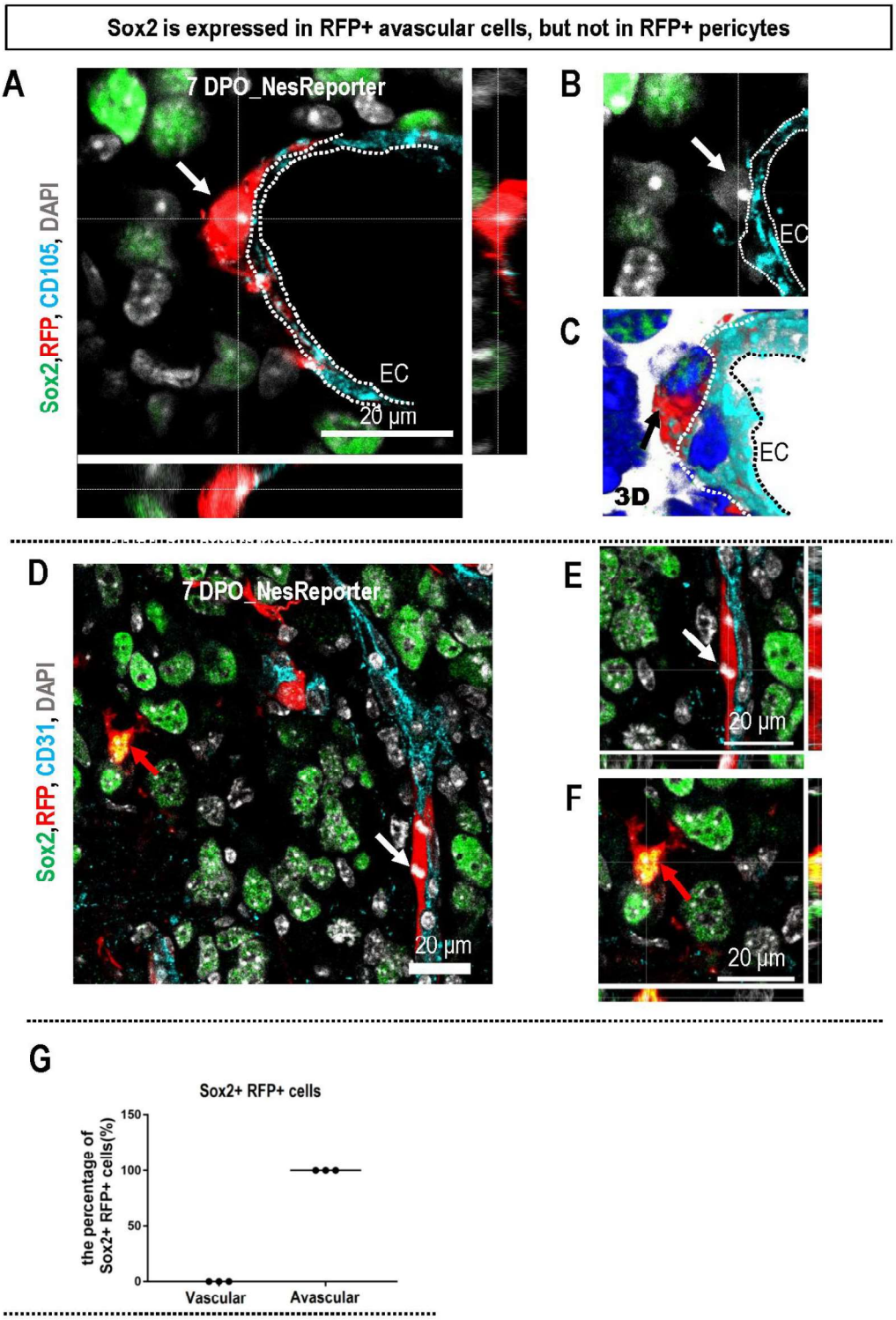

Figure-9. Sox2 is expressed in avascular RFP expressing cells, but not in vascular RFP expressing cells. (A-C) Avascular RFP expressing cells were Sox2 negative (CD105, endothelial marker). **(C)** A three-dimensional reconstructed image of a vascular RFP expressing cell which was Sox2 negative. **(D)** An overview of vascular and avascular RFP expressing cells. Vascular RFP expressing cells were Sox2 negative, while an avascular RFP expressing cell (red arrow) was Sox2 positive. **(E)** A zoom-in image of vascular RFP expressing cells (the white

arrow). **(F)** A zoom-in image of the Sox2/RFP double-expressing avascular cell (red arrow). **(G)** In 7 DPO tumors of nestin-reporter mice, all vascular RFP expressing cells were Sox2 negative and all Sox2/ RFP double-expressing cells were avascular cells. Scale bar, 20μm.

4.5 Sox2 expression in TAMEP.

In 7DPO tumors of double transgenic CX3CR1$^{GFP/+}$; nestin-reporter mice, some RFP/GFP double-positive cells expressed Sox2 (Fig. 10A). We also found Sox2/CD11b/RFP triple-positive cells in 7DPO tumors of nestin-reporter mice (Fig. 10B). In 7DPO tumors of nestin-reporter mice (Fig. 10C) the percentage of CD11b/RFP co-expressing TAMEP (as normalized to the total number of avascular RFP expressing cells) was 66.03±4.77% (n=3), and the percentage of Sox2/RFP double-expressing TAMEP of all avascular RFP expressing cells was 42.18 ± 4.43% (7DPO, n=3). These data indicated that more than 8% of avascular RFP expressing cells expressed both Sox2 and CD11b at 7DPO. The percentage of Sox2-positve avascular RFP expressing cells (in relation to avascular RFP expressing cells) was 30.43 ± 1.32% (n=3) at 14DPO and 27.26 ± 0.7% (n=3) at 21DPO. The percentage decreased during tumorigenesis, 7DPO vs 14 DPO (p=0.064), and 7DPO vs 21DPO (p=0.029).

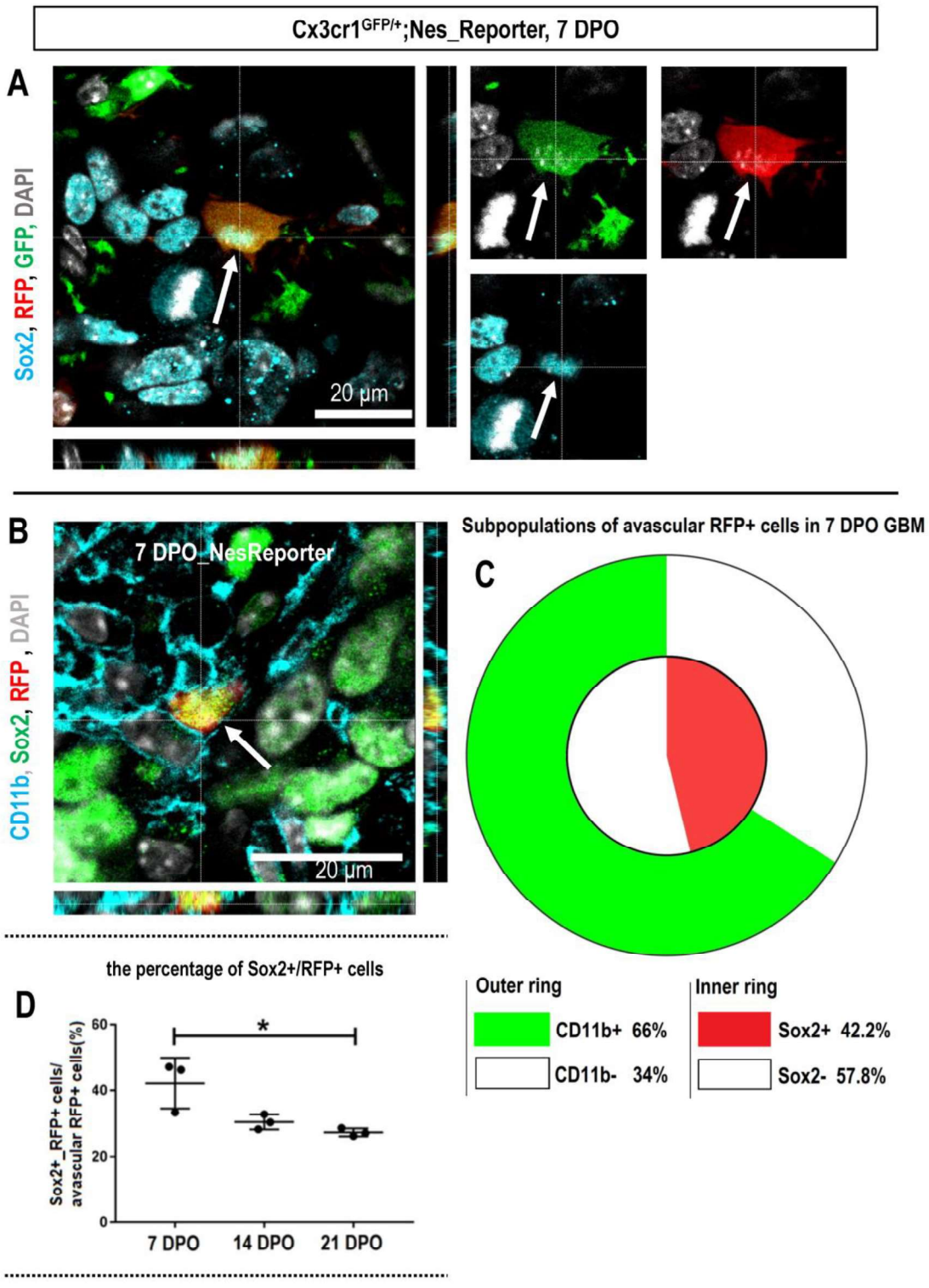

Figure-10. Sox2 expression in TAMEP. **(A)** Sox2-postive TAMEP (Sox2/RFP/GFP triple-expressing cells) in 7DPO GBM of Cx3cr1-GFP; nestin-reporter double-transgenic mice. **(B)** In 7DPO tumors of nestin-reporter mice, some TAMEP (RFP/CD11b double-expressing cells) expressed Sox2. **(C)** In 7 DPO tumors of nestin-reporter mice, 66% avascular RFP expressing cells were CD11b positive and 42.2% avascular RFP expressing cells were Sox2 positive. The overlap between these two populations were the population of Sox2/CD11b/RFP triple-positive avascular cells. **(D)** The percentage of Sox2/RFP double-expressing cells among all avascular RFP expressing cells decreased over time. Scale bar, 20μm.

4.6 Sox2/RFP double-expressinig cells are SOX2-dependent cells required for the generation of TAMEP (S2-MP)

We used $SOX2^{fl/fl}$ Nestin-reporter (SOX2-KO) double transgenic mice to knock out SOX2 in RFP expressing cells (Fig. 11A). We compared the difference in avascular/ vascular RFP expressing cell numbers at 7DPO, 14DPO and 21DPO. We observed that Sox2 was not expressed on vascular RFP expressing cells. Hence, this conditional knockout selectively affected the fraction of avascular lineage-traced cells. We used nestin-reporter mice as SOX2-wildtype controls, and iDTA; nestin-reporter (iDTA) mice as whole lineage ablation controls [67] at 21DPO.

In 7DPO tumors (Fig. 11B), the total RFP expressing cell number was 19.86 ± 1.85 (n=6) in WT mice and 14.33 ± 3.11 (n=4) in SOX2-KO animals; the vascular RFP expressing cell number was 9.56 ± 1.17 (n=6) in WT mice and 7.10 ± 1.73 (n=4) in SOX2-KO animals; the avascular RFP expressing cell number was 10.3 ± 0.78 (n=6) in WT mice and 7.24 ± 1.59 (n=4) in SOX2-KO animals.

In 14DPO tumors (Fig. 11C), the total RFP expressing cell number was 24.58 ± 4.75 (n=4) in WT mice and 6.24 ± 1.33 (n=4) in SOX2-KO animals; the vascular RFP+ cell number was 13.67 ± 3.26 (n=4) in WT mice and 4.4 ± 1.74 (n=4) in SOX2-KO animals; the avascular RFP+ cell number was 10.91 ± 3.14 (n=4) in WT mice and 2.07 ± 0.32 (n=4) in SOX2-KO animals. After conditional knockout of SOX2 in the nestin-reporter model, avascular RFP expressing cell numbers decreased very strongly at 14 DPO and vascular RFP expressing cell numbers also decreased at 14 DPO.

In 21 DPO tumors (Fig. 11D), the total RFP+ cell number was 29.78 ± 5.78 (n=5) in WT animals, 1.83 ± 0.58 (n=4) in IDTA mice respectively 12.74 ± 3.87 (n=8) after SOX2 conditional knockout; the vascular RFP expressing cell number was 27.1 ± 5.64 (n=5) in WT animals and 11.4 ± 3.76 (n=8) in SOX2-KO mice; the avascular RFP expressing cell number was 2.68 ± 0.49 (n=5) in WT animals and 1.42 ± 0.47 (n=9) after SOX2 conditional knockout. The vast majority of RFP expressing cells were ablated in IDTA mice, IDTA vs WT (p= 0.004). The population of avascular RFP+ cells was very small in WT mice at 21DPO, 9% of total RFP+ cells. Vascular RFP+ cell-numbers decreased 42% after SOX2 conditional knockout (p= 0.034).

Sox2-positive avascular RFP expressing cells made up 42% of avascular RFP expressing cells in the nestin-reporter model at 7DPO, while only 30.4% of avascular RFP-positive cells expressed Sox2 at 14DPO (Fig. 10C). After conditional knockout of SOX2 in traced cells, avascular RFP expressing cell numbers decreased very strongly at 14DPO (Fig. 11C). These results indicated that RFP/SOX2 double-labeled cells are necessary for generating Sox2-negative TAMEP (RFP/SOX2 co-expressing cells are hereafter referred to as "SOX2-dependent cells required for the generation of TAMEP"; S2-MP). As S2-MP generated Sox2-negative TAMEP within the same lineage-tracing system, these S2-MP qualify as TAMEP-progenitors.

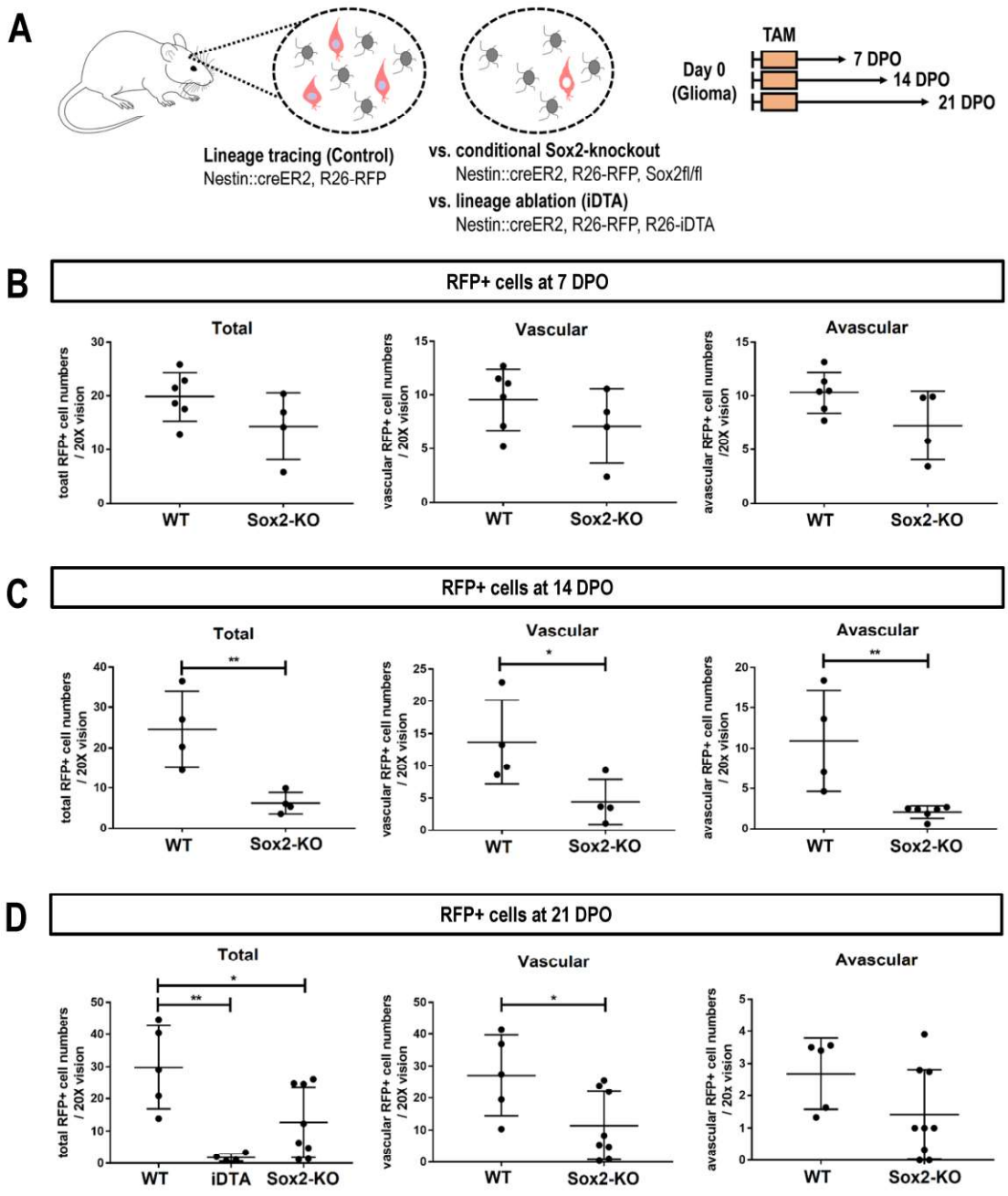

Figure-11. Sox2/RFP double-positive cells are S2-MP. (A) Nestin-reporter mice (SOX2-wildtype, WT) and SOX2-KO; nestin-reporter mice (SOX2-KO) were sub-grouped into 7DPO, 14DPO and 21DPO group, and they were inoculated with Gl261 on day 0. They were injected with tamoxifen directly after glioma inoculation. IDTA nestin-reporter mice (IDTA) were used to ablate all traced cells. **(B-C)** The quantification of vascular, avascular and total RFP expressing cells in 7/14/21 DPO tumors of WT and SOX2-KO mice. One dot on these graphs represents the average cell number of a 20x field of one mouse. **(D)** The quantification of vascular, avascular and total RFP+ cells in 7/14/21 DPO tumors of WT, IDTA, and SOX2-KO mice.

4.7 S2-MP/TAMEP do not originate from BM-derived cells

All bone-marrow derived cells of Flt3-cre:: Rosa$^{mT/mG}$ mice are labeled with GFP[80]. No Sox2-positive BM-derived cell was found in 7DPO GBM of Flt3-cre:: Rosa$^{mT/mG}$ (Fig. 12A). Monocytes and monocyte-derived macrophages can be traced in CCR2$^{GFP/+}$transgenic mice[93]. No Sox2-positive monocyte or macrophage was observed in 7DPO GBM of CCR2$^{GFP/+}$; nestin-reporter double-transgenic mice (Fig. 12B). After a lethal radiation (Fig. 12C), nestin-reporter mice were transplanted with BM cells from doner mice (Pu.1^{GFP}). Using these BM chimeric mice, we observed that all BM-derived myeloid cells (GFP expressing cells) were Sox2 negative. All these results indicated that S2-MP/TAMEP do not originate from BM-derived cells.

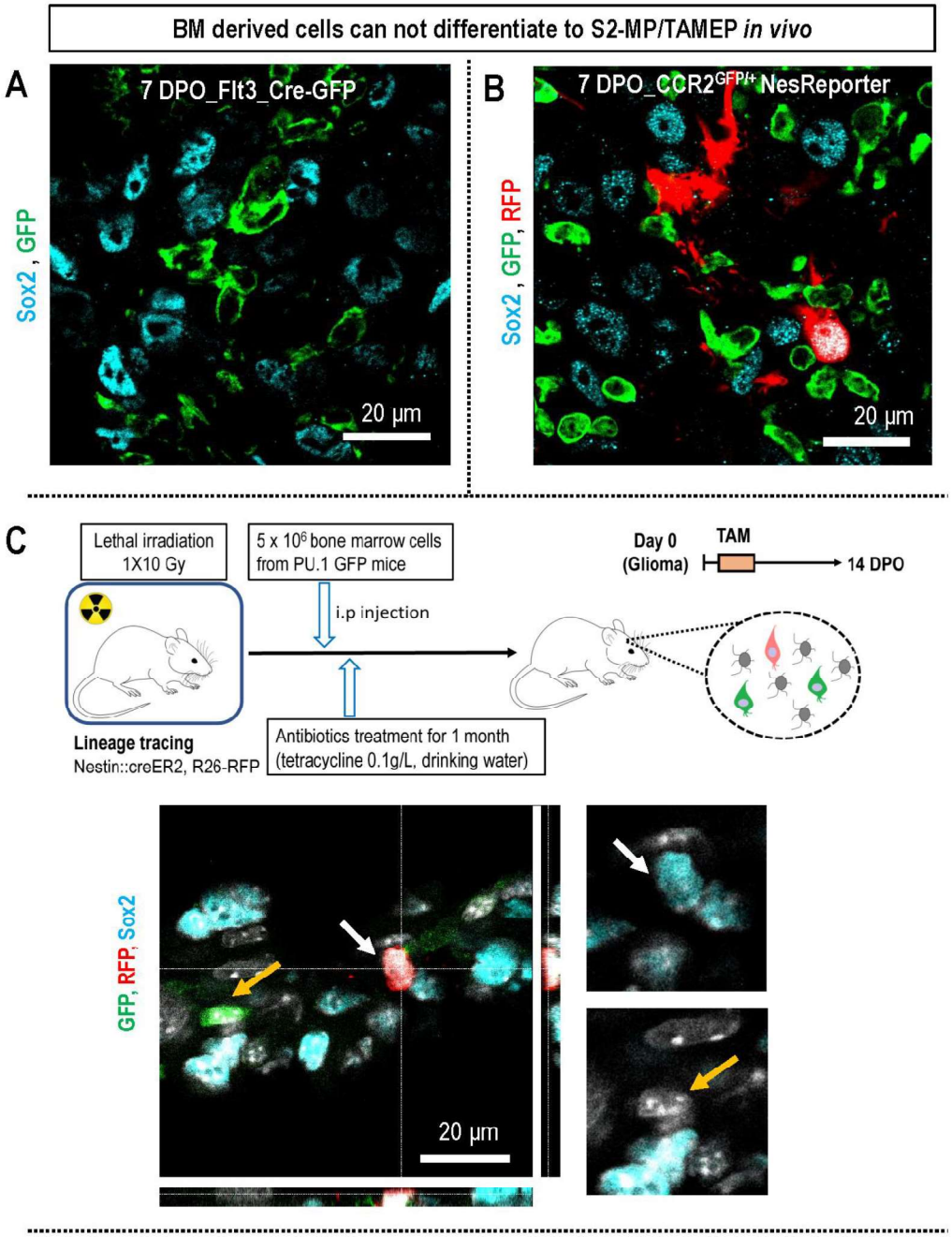

Figure-12. S2-MP/TAMEP do not originate from BM-derived cells. (A) In 7 DPO tumors of Flt3-cre:: Rosa$^{mT/mG}$ transgenic mice, BM-derived cells (GFP+) did not express Sox2. **(B)** In 7 DPO tumors of CCR2$^{GFP/+}$; nestin-reporter double-transgenic mice, monocytes and macrophages (GFP-expressing cells) did not overlap with RFP expressing cells. **(C)** BM cells were eliminated with lethal radiation in nestin-reporter mice. Then transplanted with BM cells from Pu.1^{GFP} mice to the irradiated nestin-reporter mice. In 14DPO GBM of these BM-chimeric mice, BM-derived cells (GFP+) did not express Sox2 or overlap with RFP expressing cells, while some GFP-negative RFP expressing cells expressed Sox2. Scale bar, 20µm.

4.8 S2-MP/TAMEP express the myeloid transcriptional factor Pu.1

In 7DPO GBM of nestin-reporter mice (Fig. 13A), we found a small population of avascular RFP expressing cells expressed Pu.1 and Sox2. Pu.1 is a critical myeloid and lymphoid transcription factor[77,94]. Pu.1^{GFP} transgenic mice were used to monitor myeloid cells and investigate the role of Pu.1 in the population of traced cells. Using Pu.1^{GFP}; nestin-reporter double-transgenic mice, some GFP/RFP double-expressing TAMEP were observed in 7DPO tumors (Fig. 13B), which indicated that S2-MP/TAMEP express the myeloid transcriptional factor Pu.1.

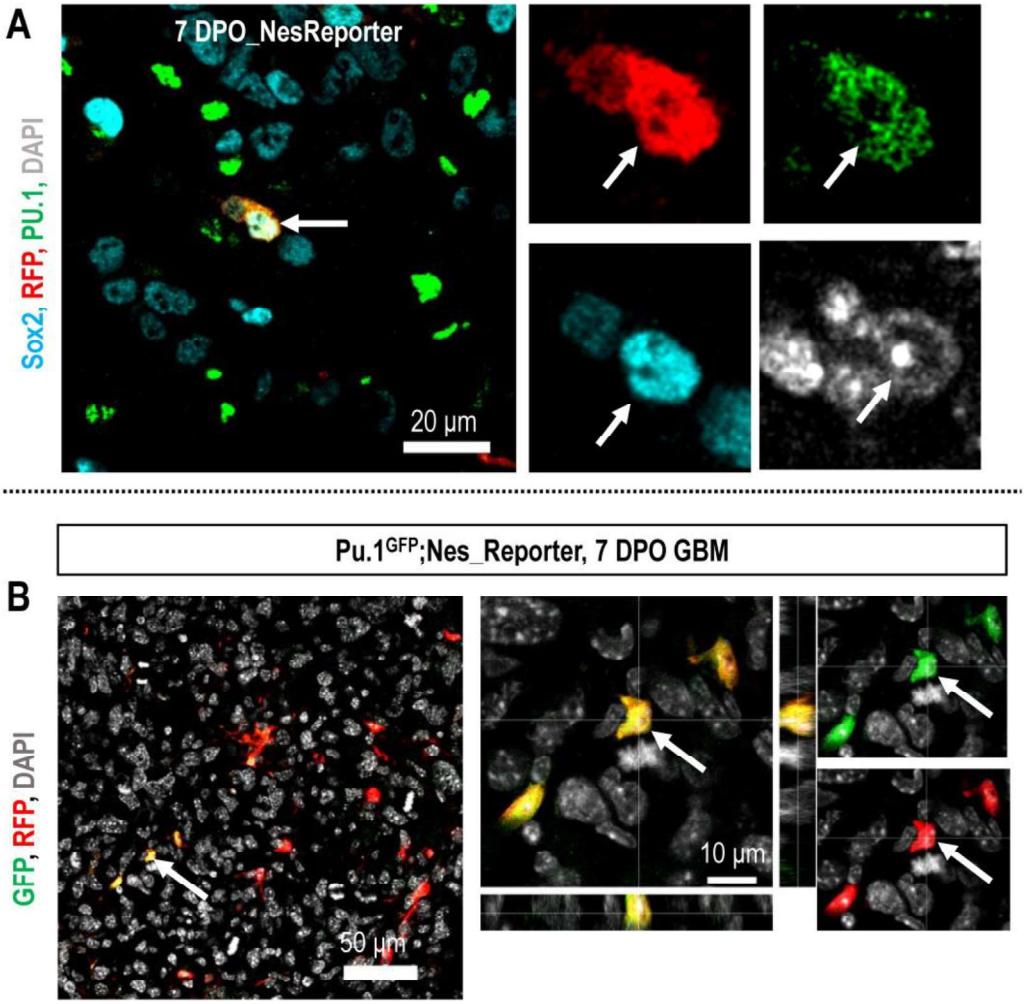

Figure-13. S2-MP/TAMEP express myeloid transcriptional factor Pu.1. (A) A small population of avascular RFP expressing cells expressed Sox2 and myeloid transcription factor Pu.1 at 7DPO. **(B)** In 7DPO tumors of Pu.1^{GFP}; nestin-reporter double-transgenic mice, some avascular RFP expressing cells overlapped with GFP expressing cells.

4.9 SOX2/PU.1 double-labelled cells in murine and human GBM

Using IHC staining of Pu.1 and Sox2 on GBM orthotopic transplantation models, Sox2/Pu.1 doubled-labelled cells were found in proneural murine GBM (Fig. 14A), classical murine GBM (Fig. 14B), classical human GBM (Fig. 14C), proneural human GBM (Fig. 14D) and another non-classified human GBM (Fig. 14E). More importantly, Sox2/Pu.1 double-labelled cells were also discovered in primary human GBM (Fig. 14F-I) and recurrent human GBM (Fig. 14J-L). All these findings indicated that these Sox2-positve myeloid cells related to GBM pathology.

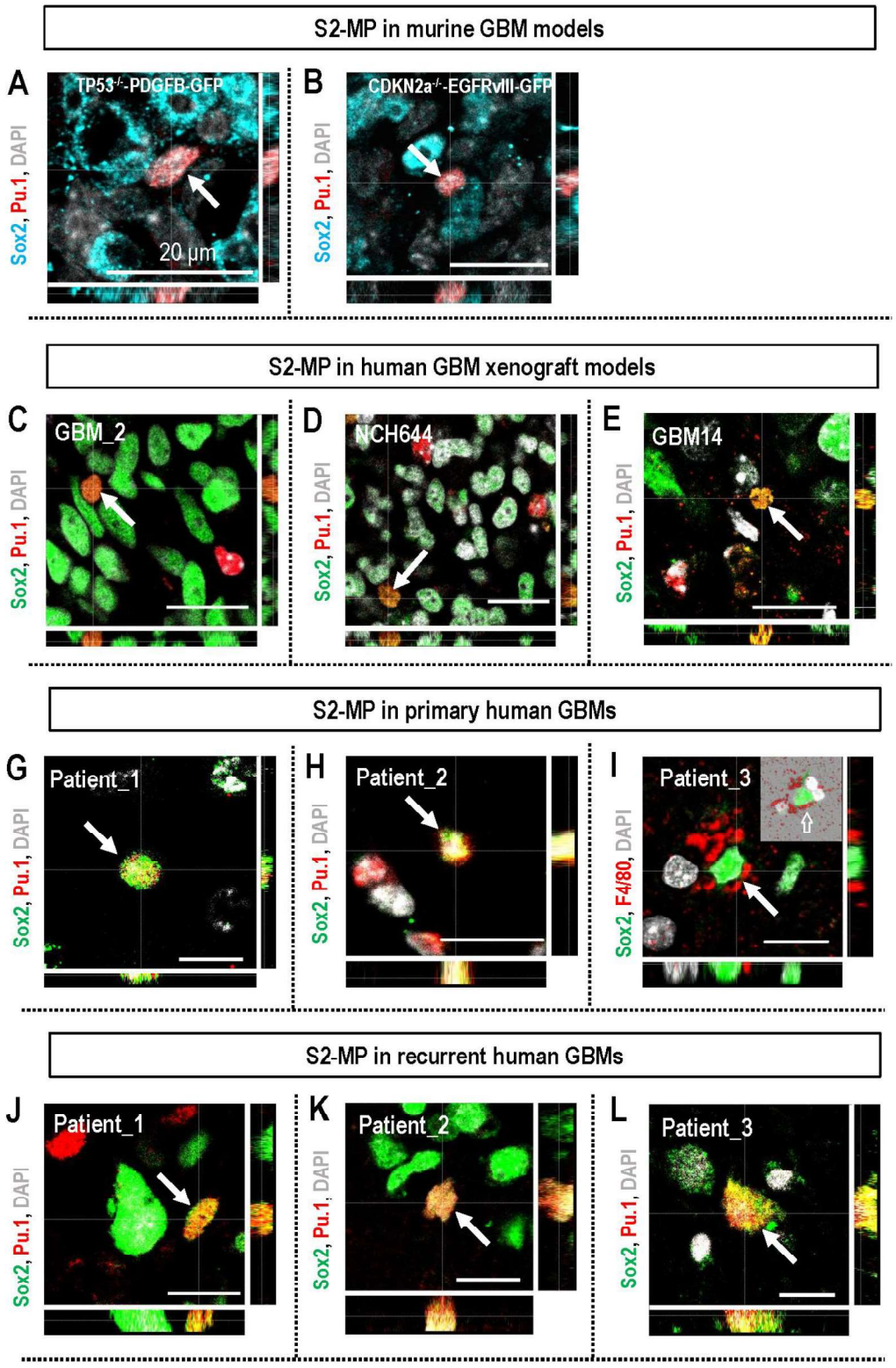

Figure-14. SOX2/PU.1 double-labelled cells in murine and human GBM. (A-B) Sox2/Pu.1 double-labelled cells in proneural murine GBM (TP53$^{-/-}$-EGFRvIII-GFP NPCs) and classical murine GBM (CDKN2a$^{-/-}$-PDGFβ-GFP NPCs). **(C-E)** Sox2/Pu.1 co-expressing cells in classical (GBM2), proneural (NCH644), and another non-classified (GBM14) human GBM xenograft models. **(G-I)** Sox2/Pu.1 double-labelled cells in primary human GBM specimens. **(J-L)** Sox2/Pu.1 double-positive cells in recurrent human GBM specimens. Scale bar, 20µm.

4.10 S2-MP/TAMEP contribute to tumor angiogenesis by promoting vessel branching in the early phase of tumorigenesis

Tumor vascular stereological analysis was performed with the spaceball method[95] in WT, SOX2-KO and IDTA mice at 7, 14 and 21DPO (Fig. 15A).To evaluate vascular complexity, average branch points were quantified to show the density of vessel branches. Vessel length density (length/spaceball-volume) and capillary length (Volume SI) were analyzed to investigate capillary length density of tumors.

In 7 DPO tumors (Fig. 15B), average branch points were 0.88 ± 0.06 (n=5) in WT animals and 0.59 ± 0.11(on=4) in SOX2-KO mice; vessel length density was 418.1 ± 28.82 mm/mm^3 (n=5) in WT mice and 291.2 ± 50.18 mm/mm^3 (n=4) after conditional knockout SOX2; capillary length was 4587 ± 293.2 mm (n=5) in WT mice and 3029 ± 906.6 mm (n=4) in SOX2-KO mice. Average branch points decreased 33% after conditional knockout of SOX2 (p=0.045).

In 14DPO tumors (Fig. 15C), average branch points were 1.1 ± 0.07 (n=4) in WT mice and 0.63 ± 0.17 (n=4) in SOX2-KO animals; vessel length density was 443.3 ± 40.41 mm/mm^3 (n=4) in WT mice and 303.1 ± 79.49 mm/mm^3 (n=4) after conditional knockout of SOX2; capillary length was 2778 ± 279.5 mm (n=4) in WT animals and 1462 ± 406.1 mm (n=4) in SOX2-KO mice. After SOX2 conditional knockout, average branch points decreased (p=0.038), and capillary length reduced too (p=0.037).

In 21DPO tumors (Fig. 15D), average branch points were 1.1 ± 0.06 (n=4) in WT animals, 0.63 ± 0.09 (n=4) after lineage ablation with IDTA model and 0.54 ± 0.06 (n=7) in SOX2-KO mice; vessel length density was 473.4 ± 33.33 mm/mm^3 (n=4) in WT mice, 277.9 ± 31.1 (n=4) in IDTA mice and 252.6 ± 33.97mm/mm^3 (n=4) in SOX2-KO animals; capillary length was 3614 ± 601.2 mm (n=4) in WT mice, 1546 ± 114.4 mm (n=4) in IDTA mice and 1068 ± 133 mm (n=7) in SOX2-KO mice. All vascular stereological data were similar in IDTA and SOX2-KO mice at 21DPO. Compared to WT mice, average branch points, vessel length density and capillary length decreased in GBM of IDTA and SOX2-KO mice at 21DPO. In 21 DPO tumors of SOX2-KO mice, tumoral-vessels had less branches and some capillaries expanded into cavernous-like vessels, which indicated that there was also a change in tumor vascular morphology after the ablation of S2-MP/TAMEP.

GBM is characterized by abundant neo-vascularization during tumor growth and progression[3]. Vessels branching is essential for tumor angiogenesis and happens in the early phase of tumorigenesis[96]. After conditional knockout of SOX2, average vessel branch points decreased at 7DPO, following with the decrease of vessel density and changes in vascular morphology at 21 DPO. These results indicated that S2-MP/TAMEP shaped tumor angiogenesis by promoting tumor vessel branching in the early phase of tumorigenesis (Fig. 15E).

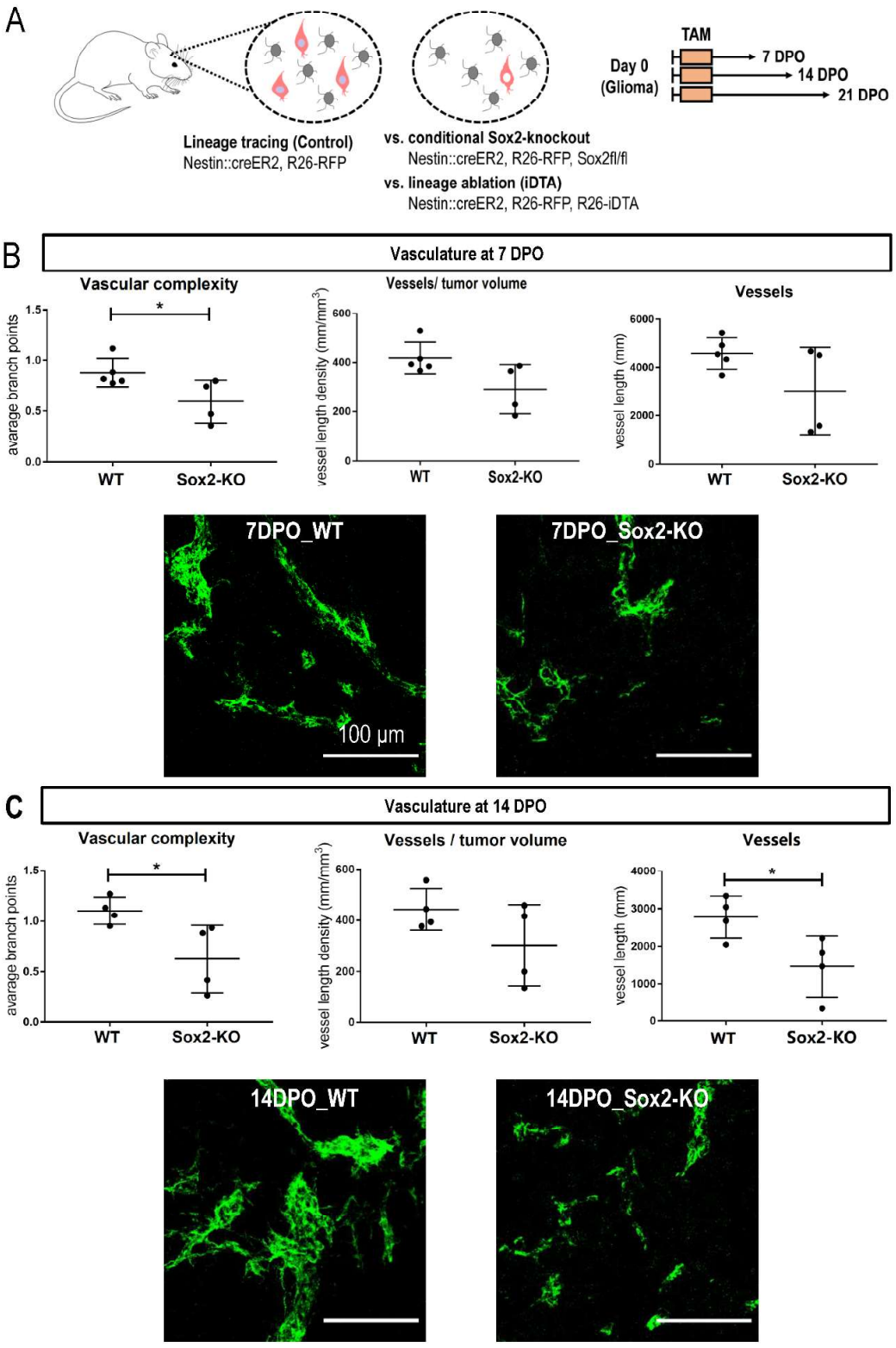

Figure-15. S2-MP/TAMEP shape tumor angiogenesis by promoting vessel branching in the early phase of tumorigenesis. (A) Experimental groups for tumor vascular stereological analysis. **(B-D)** Vascular complexity, vessels/tumor volume and vessels stereology in 7/14/21 DPO tumors of SOX2-KO and WT mice were analyzed. IDTA; nestin-reporter mice (IDTA) were used to ablated all traced cells. Each dot on these graphs represent the average data of one mouse. Representative vascular images from experimental groups were presented below

corresponding graphs: scale bar,100μm. **(B)** Comparing to WT mice, the average vessel branch points decreased in SOX2-KO mice at 7DPO. **(C)** The average vessel branch points and vessel length decreased at 14DPO after knockout of SOX2 in traced cells.

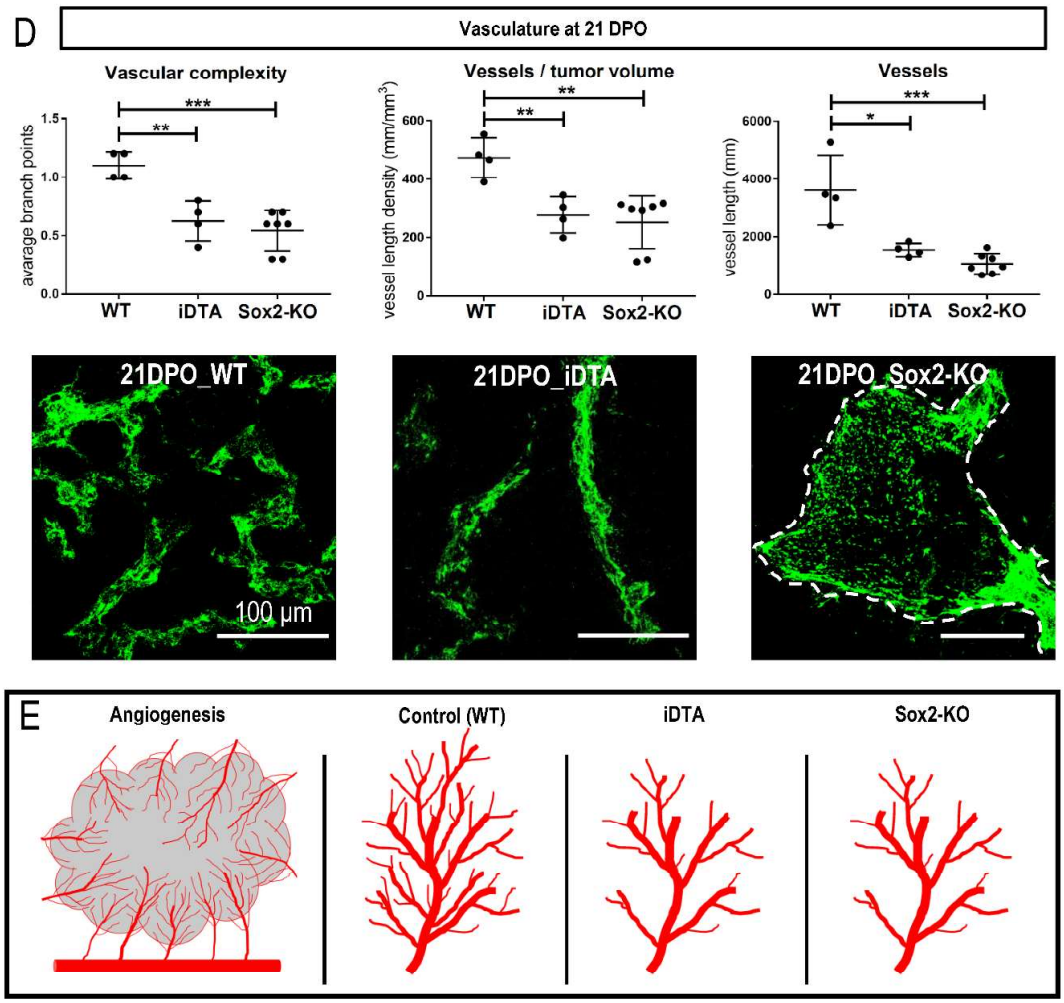

Figure-15. (D) The average vessel branch points, the vessel length, and vessel density in 21 DPD tumors diminished when SOX2 was conditional knocked out. **(E)** A graphic summary to show that tumoral vessels had less branches after avascular RFP expressing cells (S2-MP/TAMEP) were ablated in SOX2-KO and IDTA mice, which indicated that S2-MP/TAMEP promoted tumor angiogenesis by contributing to vessel branching in the early phase of tumorigenesis.

4.11 S2-MP/TAMEP control GBM expansion

To study the role of S2-MP/TAMEP in GBM expansion, we analyzed tumor volumes of WT, IDTA and SOX2-KO mice at 21 DPO (Fig. 16A). Comparing to WT mice, IDTA and SOX2-KO mice had smaller tumor size (Fig. 16B). Tumor volumes were 54.09 ± 3.83 mm^3 (n=7) in WT mice, 12.47 ± 0.8 m m^3 (n=7) in IDTA mice and 20.44 ± 1.96 mm^3 (n=10) in SOX2-KO mice (Fig. 16C). Tumor volumes decreased after lineage

ablation using the iDTA mice ($p<0.0001$). Similarly, tumor volumes decreased after the ablation of S2-MP/TAMEP in SOX2-KO mice ($p<0.0001$), which indicated that S2-MP/TAMEP controlled the GBM expansion.

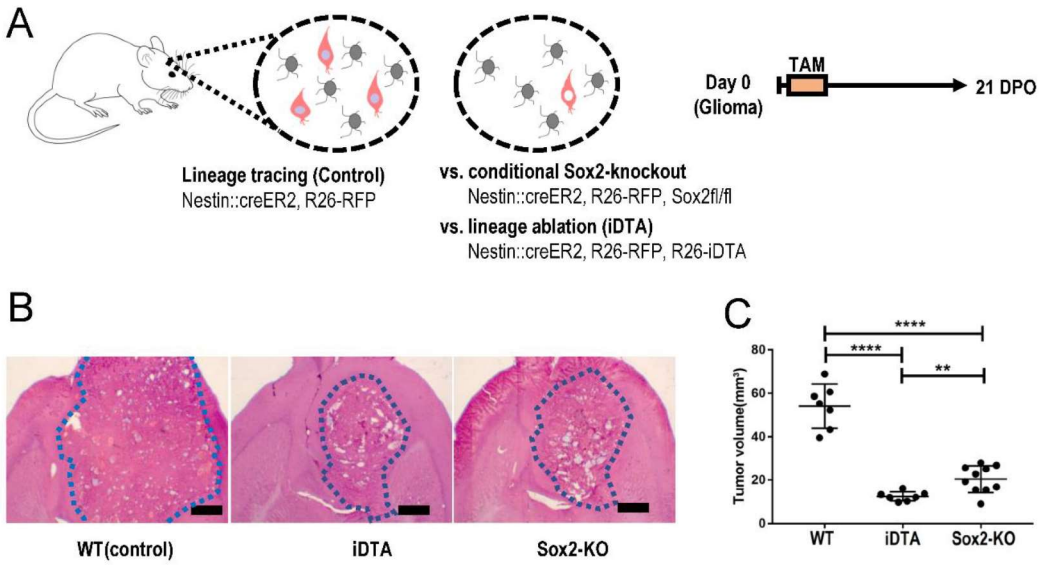

Figure-16. S2-MP/TAMEP control the GBM expansion. (A) 21DPO tumor volumes were analyzed in nestin-reporter mice (WT control), iDTA mice (lineage ablation) and SOX2-KO mice (conditional knockout of SOX2 in traced cells). **(B)** Representive tumoral images with HE-staining of each group. Scale bar, 1 cm. **(C)** Tumor volumes of WT, IDTA, and SOX2-KO mice: tumor volumes decreased after lineage ablattion in iDTA mice; tumor volumes reduction were also obtained after conditional knockout of SOX2 (S2-MP/TAMEP were ablated while vascular cells were not), indicating that S2-MP/TAMEP controlled the GBM expansion.

4.12 S2-MP/TAMEP and pericytes originated from cells on meninges.

Using IHC staining of laminin for locating the leptomeninges[97], some RFP expressing cells were found on the meninges of nestin-reporter mice (Fig. 17A). After dissecting whole-mount meninges[83] from 7DPO nestin-reporter mice (Fig. 17B), lots of RFP cells were observed on the venous sinus of meninges (Fig. 17B-E). Some of these meninx RFP expressing cells could be labeled with Sox2 (Fig. 17D-E) and most of them located on the confluence of sinuses (Fig. 17E).

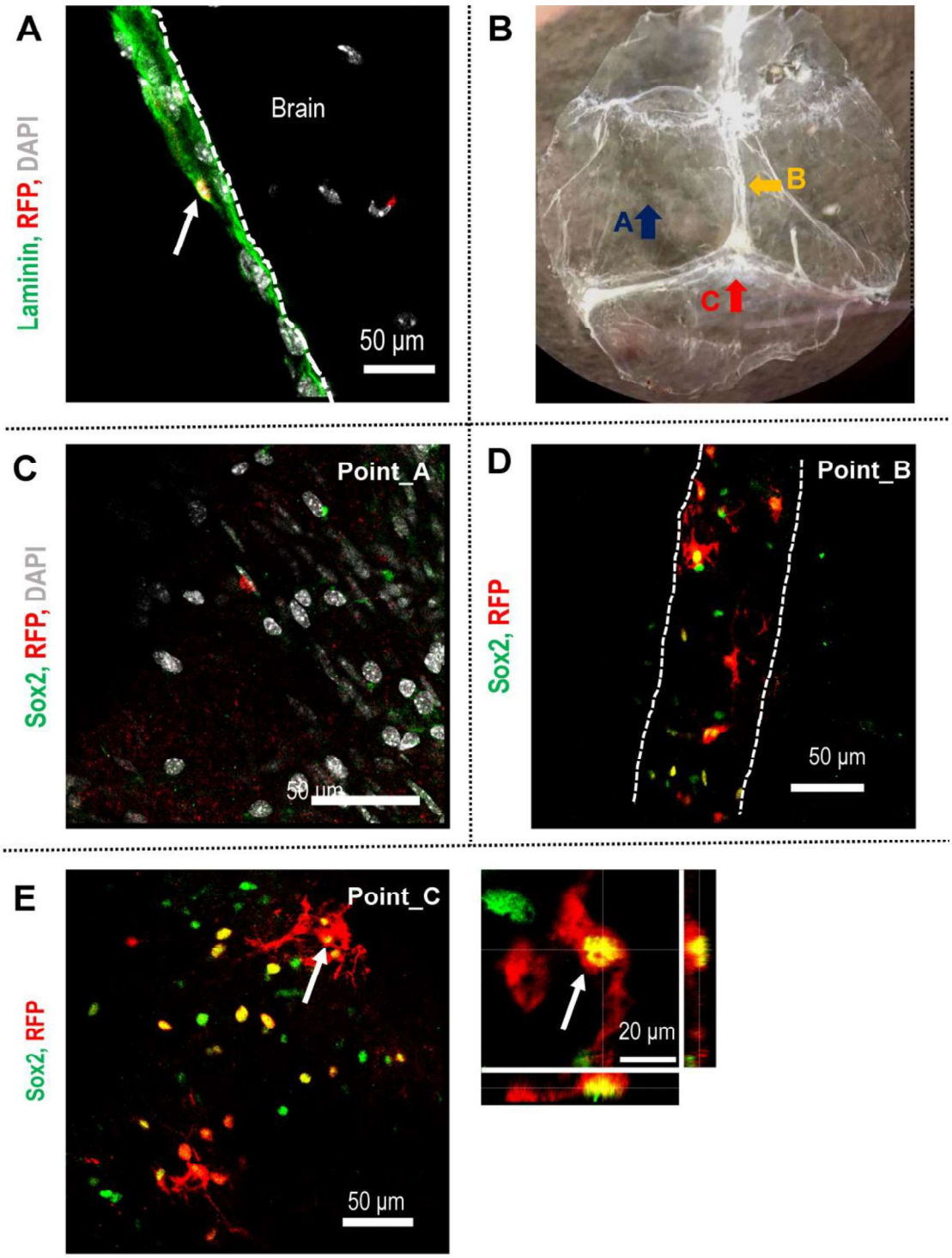

Figure-17. RFP expressing cells on the meninges of nestin-reporter mice. (**A**) An RFP expressing cell (white arrow) on the leptomeninges (laminin). (**B**) Mouse whole-mount meninges were dissected. Selected points on meninges of nestin-reporter mice: point-A, on the sinus-free meninx; point-B, on the superior sagittal sinus; point-C, on the confluence of sinuses. (**C**) Few cells expressed RFP or Sox2 at point-A. (**D**) Cells expressed RFP and Sox2 at point B. (**E**) Many Sox2/RFP co-expressing cells located at point C. The superior sagittal sinus was demarcated with white dashed lines.

We isolated cells from meninges of newborn double transgenic Cx3cr1$^{GFP/+}$; nestin-reporter mice and then transplanted these cells with GBM cells to the brain of athymic nude mice (Fig. 18A). RFP expressing cells were found in 7DPO tumors after tamoxifen injection (Fig. 18B-C). Some avascular RFP expressing cells were co-labeled with CX3CR1-GFP (Fig. 18B) and some RFP expressing cells shared pericyte marker (Fig. 18C), which may open the possibility that TAMEP and RFP-expressing pericytes originate from cells on the meninges.

Collectively, we uncovered that the meninges may be one potential source for S2-MP/TAMEP and RFP+ pericytes.

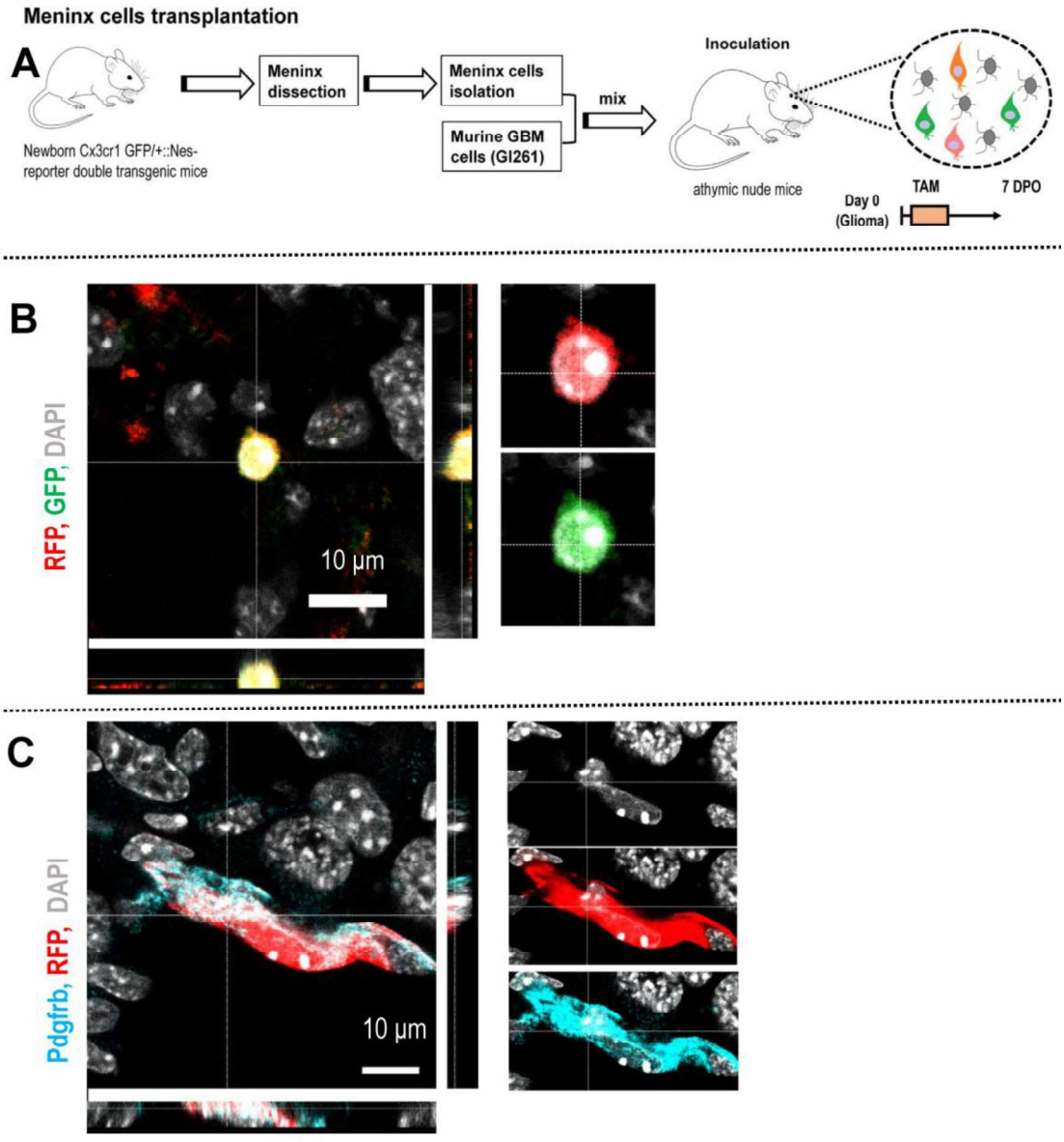

Figure-18. S2-MP/TAMEP and traced tumoral pericytes originated from cells on meninges. (**A**) Meninges of newborn Cx3cr1$^{GFP/+}$; nestin-reporter mice were dissected and digested into single cells. Mixed these cells with Gl261 cells and transplanted them into nude mice. Mice were injected with tamoxifen and perfused at 7DPO. (**B**)

avascular RFP expressing cells expressed GFP and these double-expressing cells were TAMEP. (**C**) vascular RFP expressing cells expressed pericyte marker PDGFR-β.

5. Discussion

Using a nestin-reporter transgenic mouse strain, we have monitored a lineage of GBM-induced tumor-parenchymal cells. Different from other nestin-reporter mice[98], these traced cells appeared in the tumor center from the early stage of tumorigenesis. According to their relationships with vessels[35], we subgrouped them into two populations, vascular RFP expressing cells and avascular RFP expressing cells.

We identified vascular RFP expressing cells are pericytes according to their juxtaposition with endothelial cells and expression of pericyte markers[34,35,53,99]. These pathological pericytes were generated during tumor growth and many of them were proliferative. It was reported previously that monocytes could differentiate to pericytes[100], but our traced pericytes did not express any myeloid cell marker according to IHC analysis. Using a monocyte reporter[101,102] ($CCR2^{GFP/+}$; nestin-reporter), we further documented that our traced pericytes did not overlap with monocytes. Pericytes have multi-potency similar to mesenchymal stem cells[33-35]. While recently, Guimaraes-Camboa N et al. challenged this viewpoint and suggested that pericytes would not behave as mesenchymal stem cells *in vivo* [103]. In our environments with a pathological model, we did not find any RFP expressing pericytes sharing mesenchymal stem cell markers either.

Cheng et al. reported that most pericytes in the GBM microenvironment originated from glioma stem cells[86]. In our xenografting tumor models, RFP expressing pericytes constituted a large portion of the pericyte pool in GBM and all RFP expressing pericytes were necessarily of host-origin as these pericytes expressed host-derived red fluorescent protein while GBM cells did not carry any inheritable fluorescence. With PDGFR-β /IDH1-R132H double-IHC staining on IDHI-R132H mutant human GBM specimens, we found many PDGFR-β expressing cells. However, these were never labeled for the clonal tumor marker IDHI-R132H. Collectively, we found that the majority of intratumoral pericytes in GBM were of host-derived.

Pericytes are believed to be key regulators in brain vascular homeostasis[33-35,53]. In this study, we monitored a population of pericytes which was of host-derived and abundant in the GBM environment. In the future, we can investigate the function of intratumoral pericytes using the nestin-reporter model (now established). We can study their roles

on tumor angiogenesis and their contributions to the blood tumor/brain barrier[48]. As pericytes participate in pathological processes of many different CNS diseases[33,48], it is also interesting to investigate their roles in models for stroke [49], epilepsy [50] or spinal cord injury [51].

Avascular RFP expressing cells could not be labeled with pericyte markers[35] (PDGFR-β, Desmin, NG2, CD248, and CD146), mesenchymal stem cell markers (CD29, Sca1,CD105, CD44), mature and immature neuronal markers (Tuj1, PSA-NCAM, DCX, NeuN), oligodendrocyte markers (CNPase, MBP), or astrocyte markers (GFAP, S100B). Avascular RFP expressing cells shared myeloid markers CD11b, Cx3cr1, F4/80[23,78,101] and the myeloid transcription factor Pu.1[104], while they could not be labeled with macrophage markers CCR2 and CD45[55,101]. Uniquely, they were Iba1-negative, which is surprising as Iba1 is a marker for all microglia and CNS macrophages[78]. Altogether, this information indicates that TAMEP represent a small population of tumor-associated cells which do not fully overlap with established populations of myeloid cells.

Remarkably, some TAMEP expressed the stem cell-related transcription factor SOX2[92], while Sox2-postive myeloid cells were only observed in leukemic diseases[105]. We also found that Sox2 was expressed in avascular RFP expressing cells but not in vascular RFP expressing cells. The percentage of Sox2/RFP double-expressing cells of avascular RFP expressing cells decreased over time. At 7DPO, some Sox2/RFP co-expressing cells shared the myeloid markers CD11b and Cx3cr1. Conditional knockout of SOX2 in the nestin-reporter model induced a very large reduction in the total number of RFP expressing avascular cells (at 14 DPO). Since the SOX2/RFP co-expressing avascular cells represent only 30% to 40% of all avascular RFP expressing cells and since the SOX2-KO affected a much larger population, which must include also SOX2-negative cells, we conclude that SOX2/RFP co-expressing cells are SOX2-dependent cells required for the generation of TAMEP (S2-MP). As S2-MP generated TAMEP within the same lineage-tracing system, these S2-MP qualify as direct precursor cells of TAMEP.

Some S2-MP expressed the myeloid transcription factor Pu.1[77,94] at 7DPO by using Pu.1^{GFP}; nestin-reporter double-transgenic mice or immunostaining Pu.1 in the nestin-reporter model. These Pu.1/Sox2 double-labeled cells represent cells in transition from

the S2-MP to the TAMEP stage. However, no BM-derived cells or Iba1-positive myeloid cells can be labeled with Sox2. Collectively, this information indicates that Sox2/ Pu.1 can be used as double-markers for the detection of the non-canonical myeloid-like cells (S2-MP/TAMEP). As GBM is characterized by its high heterogeneity[5,14-17], we also investigated whether S2-MP/TAMEP existed in different subtypes of GBM. Using IHC staining of Sox2/Pu.1 in GBM implantation models, we found S2-MP/TAMEP in proneural murine GBM, classical murine GBM, proneural murine GBM, classical human GBM, proneural human GBM and non-classified human GBM. In brief, we uncovered that S2-MP/TAMEP existed in different genetic GBM subtypes. Next, we also demonstrated that Sox2/Pu.1 double-expressing cells existed in primary or recurrent human GBM specimens. We found Sox2/Pu.1 double-expressing cells were rare in primary human GBM and it was more difficult to find them in primary human GBM than in recurrent human GBM. One explanation for the small number of Sox2/Pu.1 double-expressing cells in primary human GBM is that the tumor specimens were obtained several years after GBM formation, while S2-MP/TAMEP were abundant only in the early stage of GBM (7DPO and 14DPO) and diminished at 21DPO in nestin-reporter mice.

After conditional knockout of SOX2 in the nestin-reporter model (S2-MP/TAMEP number decreased), tumor vessel density was reduced significantly at 14DPO and 21DPO. As Sox2 was exclusively expressed in S2-MP, we could conclude that it was S2-MP/TAMEP but not traced pericytes playing key roles in promoting tumor angiogenesis. Vessel sprouting happens during the early stage of tumorigenesis and vessel branching is essential to the GBM neo-vascularization[96]. The population of S2-MP/TAMEP was large at 7DPO and less vessel branches were in SOX2-KO mice at 7/14/21DPO. This information indicates that S2-MP/TAMEP play a key role in promoting the GBM vessel-sprouting in the early stage of tumorigenesis. Furthermore, tumor vascular morphology was also affected and tumor volumes decreased largely at 21DPO after conditional knockout of SOX2. Altogether, S2-MP/TAMEP shaped tumor vascularization in the early stage of GBM and controlled GBM expansion (Fig.19).

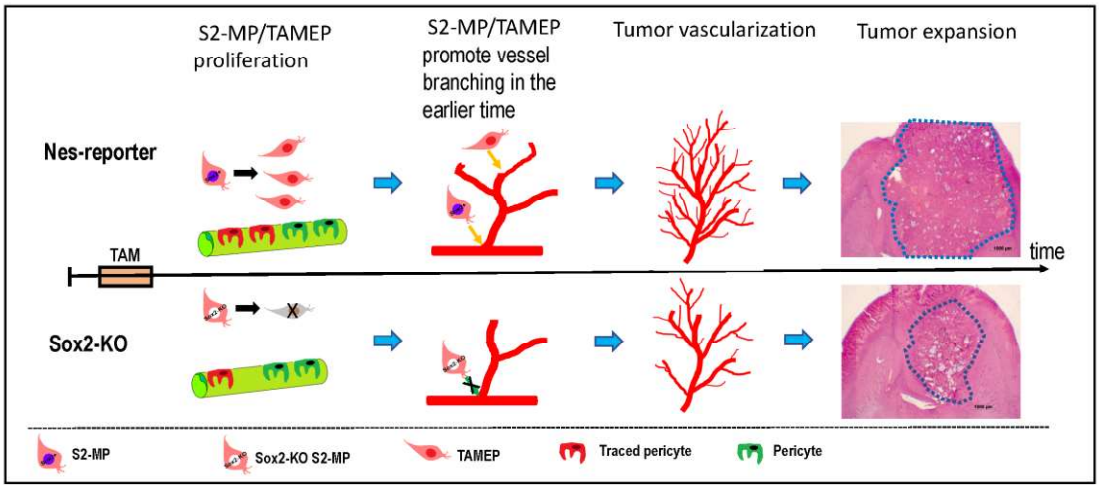

Figure-19. A summary of the function of S2-MP/TAMEP. After conditional knockout of SOX2, S2-MP were ablated and fewer TAMEP were generated. The ablation of S2-MP/TAMEP affected tumor vessel branching in the early phase of GBM angiogenesis, resulting in the reduction of tumor vascularization and smaller tumors.

TAM originate from parenchymal microglia and invading monocyte-derived macrophages[23,78,101,106]. Comparing to microglia and macrophages, S2-MP/TAMEP had an atypical expression profile: S2-MP/TAMEP were Iba1-negative; the immunofluorescence inspection on TAMEP with IHC staining of CD11b was similar to physiological microglia and much weaker than TAM; TAMEP expressed Sox2, which was never described in TAM before[23,78,101,106]. We documented that S2-MP/TAMEP were not monocytes or macrophages as no S2-MP/TAMEP shared monocyte/macrophage markers[101] CD45 and CCR2. We also demonstrated that BM-derived cells were not the source of S2-MP/TAMEP by using BM-chimeric mice. Another evidence to support this conclusion is that no BM-derived cells in GBM microenvironment expressed Sox2 (using Flt3-cre; Rosa$^{mT/mG}$ transgenic mice). All this information indicated that we uncovered a small population of parenchymal tumor-associated cells (TAMEP) and their progenitors (S2-MP) which can shape tumor neo-vascularization in the early stage of GBM and control GBM expansion. Targeting these newly identified S2-MP/TAMEP will be highly promising for developing novel anti-angiogenesis therapies of GBM.

Surprisingly, we found RFP expressing cells on adult mouse meninges and some of them expressed Sox2. Most of Sox2/RFP double-expressing cells were concentrated on the confluence of sinuses. Xenografting cells isolated from meninges of newborn

Cx3cr1$^{GFP/+}$; nestin-reporter mice together with glioma cells to nude mice, we uncovered RFP expressing cells in 7DPO GBM. Some RFP expressing cells co-labeled with Cx3cr1-GFP, which indicated that these GFP/RFP co-expressing cells were TAMEP, and these TAMEP originated from cells of the meninges. Some RFP expressing cells were identified as pericytes by using IHC staining for pericyte marker PDGFR-β, which indicated that RFP expressing pericytes could also derive from the meninges. However, it should be noted that these co-transplantation experiments were performed with cells isolated from meninges of newborn mice. We still need more evidence to prove that cells on meninges of adult mice could also generate TAMEP and pericytes and play a role in tumor angiogenesis. Anyway, we found many Sox2/RFP co-expressing cells on adult murine meninges and these Sox2/RFP double-positive cells might be precursors of S2-MP/TAMEP. We are the first to report meninges-derived S2-MP/TAMEP and meningeal pericytes contributing to the pathological environment of GBM. Further investigation on the migration and the differentiation mechanism of meninx-derived S2-MP/TAMEP and meningeal pericytes may indicate new targets for GBM therapy. Eliminating their potential precursors on the meninges, like precise radiotherapy, can represent new strategy for GBM radiotherapy.

6. Summary

In this study, we monitored and identified three intratumoral cell-populations: pericytes, S2-MP and TAMEP.

Traced (RFP+) pericytes expressed the pericyte markers PDGFR-β, Desmin, NG2, CD146 and CD248[33,35]. RFP+ pericytes did not share any myeloid or mesenchymal stem cell markers, and they did not originate from the bone marrow, monocyte or mesenchymal stem cells. These host-derived pericytes were highly proliferative and abundant in advanced GBM. As pericytes play important roles in maintaining the CNS vascular homeostasis[34], these traced host-derived pericytes are promising regulators of the blood brain/tumor barrier.

We uncovered a new population of tumor-associated cells with an atypical expression profile of myeloid markers (TAMEP): they expressed the myeloid markers CD11b, CX3CR1, F4/80 and the myeloid transcription factor Pu.1; they could not be labeled with the macrophage marker CD45 or CCR2[22,101]; they were atypical because they did not express Iba1 which is a canonical marker for all microglia and CNS macrophages[78]. It is striking that we found some TAMEP that expressed the stem-cell transcription factor Sox2. This is the first report on Sox2-positive myeloid-like cells in GBM, as Sox2-positive myeloid cells were otherwise only observed in leukemia[105]. We found that Sox2/RFP co-expressing cells were required for the generation of TAMEP since TAMEP were ablated at 14DPO after conditional knockout of SOX2 in nestin-reporter models. Hence, we termed this subpopulation of traced GBM microenvironmental cells Sox2-dependent cells required for the generation of TAMEP (S2-MP). We explored the origin of S2-MP/TAMEP and found that they were not derived from monocytes, mesenchymal stem cells or BM cells. We observed some Sox2/Pu.1 co-expressing TAMEP in 7DPO GBM of nestin-reporter models, and these Sox2/Pu.1 co-expressing cells were interpreted to represent cells in transition from the S2-MP to the TAMEP stage. As Iba1-positive TAM (which can express PU.1) are always Sox2-negative[107-109], we can use Sox2/Pu.1 as double-markers to identify S2-MP/TAMEP. Next, Sox2/Pu.1 co-expressing cells were found in different genetic GBM subtypes as well as in primary and recurrent human GBM specimens, indicating that S2-MP/TAMEP widely existed in murine and human GBM.

6. Summary

After conditional knockout of SOX2 in nestin-reporter models, tumor vessel density and tumor volumes decreased drastically at 21DPO. As Sox2 was exclusively expressed in S2-MP and since S2-MP/TAMEP were ablated in the SOX2-KO; nestin-reporter models at 14DPO, we can conclude that S2-MP/TAMEP promoted tumor angiogenesis and expansion. Furthermore, we found tumor vessel branching and vessel morphology was also altered at 21DPO in the SOX2-KO model. All this information indicates that S2-MP/TAMEP shaped tumor neo-vascularization and controlled GBM expansion by promoting vessel sprouting in the early stage of tumorigenesis. Targeting S2-MP/TAMEP will be highly promising for developing novel anti-angiogenesis therapies of GBM.

Furthermore, we documented that GBM-initiated S2-MP/TAMEP and RFP expressing pericytes might originate from cells on meninges, offering a S2-MP/TAMEP directed therapeutic strategy by irradiation of selected meningeal areas.

Zusammenfassung

Das Glioblastom (GBM) ist der häufigste und aggressivste primäre Gehirntumor. GBM-Zellen sind von der lokalen Tumorumgebung abhängig, dessen Haupkomponenten aus Gefäßzellen sowie tumorassoziierten myeloiden Zellen (TAM) bestehen. TAM setzen sich aus Mikroglia und peripheren Makrophagen zusammen und unterstützen sowohl die Invasion von GBM-Zellen wie auch die Ausbildung eines neuen Gefäßnetzwerks im Tumor. Dessen Architektur und Permeabilität wird dabei massgebend durch Perizyten reguliert, die einen wichtigen Teil der neurovaskulären Funktionseinheit des Gehirn bilden[35].

Im Rahmen meiner medizinischen Doktorarbeit habe ich ein neues Gliom-Maus-Modell verwendet um genetisch markierte Zelllinien im Tumor-Parenchym- (in Nestin-creER2, R26-tdTomato Mäusen; abgekürzt als Nestin-Reporter-Mäuse) zu verfolgen. Bei der Betrachtung dieses Modells beobachtete ich, dass zwei verschiedene Zelltypen den genetischen Reporter exprimierten: tumorassoziierte Gefäßzellen, die sich als reife Perizyte herausstellten, sowie tumorassoziierte Zellen ohne direkten Gefäßbezug, die sich als eine neue Art von lokalen myeloiden Vorläuferzellen herausstellten, die vorübergehend während des Wachstums von Glioblastomen auftraten.

Durch eine detaillierte Immunfluoreszenzanalyse fand ich heraus, dass die erste Population von markierten (tdTomato +) Gefäßzellen eng mit Endothelien assoziiert war und durch eine Reihe von Markern wie PDGFR-β, Desmin, NG2, CD146 und CD248 als Perizyten identifiziert werden konnten [33,35]. Diese Perizyten waren stark proliferativ und breiteten sich über die gesamte Neovaskulatur des murinen GBMs aus.

Die zweite Population genetisch markierter (tdTomato+) Zellen erwies sich als eine zuvor nicht beschriebene Population von Tumor-assoziierten Zellen mit einem myeloiden Expressions-Profil (TAMEP). Unter Verwednugn von verschiedenen transgenen Mausstämmen (Pu1-GFP-, CCR2-GFP- und CX3CR1-GFP-Mäuse) und Knochenmarks-Chimären (mittels nestin-creER2, R26-tdTomato- und Pu1-GFP-Mäusen) haben wir den Ursprung dieser Zellen untersucht. Zusätzlich wurden diese neuartigen Zellen in diesen Mausmodellen mittels Immunfluoreszenz charakterisiert und erwiesen sich unter anderem als positiv für die myeloidcen Zellmarker CD11b und F4/80, jedoch als negativ für Iba1, CD45 und CCR2. Somit zeigten diese Tumor-

assoziierten Zellen eine auffallende Ähnlichkeit mit Mikroglia, sie unterschieden sich jedoch von TAM, da sie keinen mikroglialen Ursprung haben und nicht aus dem Knochenmark kommen. Bemerkenswerterweise stammen diese genetisch markierten Zellen von einer lokalen Vorläuferzelle ab, die in der Homöostasesituation inaktiv ist. Höchst interessant dabei war, dass einige TAMEP den stammzelleigenen Transkriptionsfaktor Sox2 exprimierten. Dies ist das erste Mal, dass Sox2-positive myeloide Zellen in GBM beschrieben werden, da Sox2-positive myeloide Zellen ansonsten bisher nur während einer Leukämie [105] beobachtet wurden. Die Induktion eines orthotopen GBMs im Nestin-Reporter-Modell aktivierte diese SOX2-abhängige Vorläuferzellpopulation. Die Depletion dieser Vorläuferzellpopulation in konditionellen Sox2-Knockout-Mäusen entfernte die gesamte Untergruppe der beobachteten Zellen mit einem myeloiden Expressionsprofil (TAMEP). Die histopathologische Untersuchung ergab, dass eine kleine Sox2-positive Untergruppe von TAMEP einen großen Einfluss auf den Krankheitsverlauf hat, indem sie die Vaskularisierung und Größe des Glioblastoms kontrolliert. Schließlich habe ich kombinierte Immunfärbung für PU.1 und SOX2 an menschlichen GBM-Proben angewendet und konnte unsere neu identifizierten tumorassoziierten myeloiden Vorläuferzellen in verschiedenen Proben humaner GBM nachweisen.

Zusammengenommen legen unsere Daten nahe, dass ruhende Vorläufer TAMEP (Zellen, die myeloide Marker exprimieren, aber keinen myeloiden Ursprung haben) erzeugen, welche tiefgreifende neuroonkologische Auswirkungen haben und damit ein neues und vielversprechendes therapeutisches Ziel darstellen, um das anti-angiogene Regime bei GBM zu unterstützen.

7. References

1. De Backer A. Handbook of neurosurgery, 8th edition. *Acta Chir Belg* 2016; **116**(4): 269.
2. Leece R, Xu J, Ostrom QT, Chen Y, Kruchko C, Barnholtz-Sloan JS. Global incidence of malignant brain and other central nervous system tumors by histology, 2003-2007. *Neuro Oncol* 2017; **19**(11): 1553-64.
3. Norden AD, Drappatz J, Wen PY. Novel anti-angiogenic therapies for malignant gliomas. *Lancet Neurol* 2008; **7**(12): 1152-60.
4. Weller M, van den Bent M, Tonn JC, et al. European Association for Neuro-Oncology (EANO) guideline on the diagnosis and treatment of adult astrocytic and oligodendroglial gliomas. *Lancet Oncol* 2017; **18**(6): e315-e29.
5. Verhaak RG, Hoadley KA, Purdom E, et al. Integrated genomic analysis identifies clinically relevant subtypes of glioblastoma characterized by abnormalities in PDGFRA, IDH1, EGFR, and NF1. *Cancer Cell* 2010; **17**(1): 98-110.
6. Cancer Genome Atlas Research N. Comprehensive genomic characterization defines human glioblastoma genes and core pathways. *Nature* 2008; **455**(7216): 1061-8.
7. Chow LM, Endersby R, Zhu X, et al. Cooperativity within and among Pten, p53, and Rb pathways induces high-grade astrocytoma in adult brain. *Cancer Cell* 2011; **19**(3): 305-16.
8. Frattini V, Trifonov V, Chan JM, et al. The integrated landscape of driver genomic alterations in glioblastoma. *Nat Genet* 2013; **45**(10): 1141-9.
9. Brennan CW, Verhaak RG, McKenna A, et al. The somatic genomic landscape of glioblastoma. *Cell* 2013; **155**(2): 462-77.
10. Weller M, Pfister SM, Wick W, Hegi ME, Reifenberger G, Stupp R. Molecular neuro-oncology in clinical practice: a new horizon. *Lancet Oncol* 2013; **14**(9): e370-9.
11. van den Bent MJ, Weller M, Wen PY, Kros JM, Aldape K, Chang S. A clinical perspective on the 2016 WHO brain tumor classification and routine molecular diagnostics. *Neuro Oncol* 2017; **19**(5): 614-24.
12. Lapointe S, Perry A, Butowski NA. Primary brain tumours in adults. *Lancet* 2018; **392**(10145): 432-46.
13. Stupp R, Mason WP, van den Bent MJ, et al. Radiotherapy plus concomitant and adjuvant temozolomide for glioblastoma. *N Engl J Med* 2005; **352**(10): 987-96.
14. Broekman ML, Maas SLN, Abels ER, Mempel TR, Krichevsky AM, Breakefield XO. Multidimensional communication in the microenvirons of glioblastoma. *Nat Rev Neurol* 2018; **14**(8): 482-95.
15. Patel AP, Tirosh I, Trombetta JJ, et al. Single-cell RNA-seq highlights intratumoral heterogeneity in primary glioblastoma. *Science* 2014; **344**(6190): 1396-401.
16. Puchalski RB, Shah N, Miller J, et al. An anatomic transcriptional atlas of human glioblastoma. *Science* 2018; **360**(6389): 660-3.
17. Behnan J, Finocchiaro G, Hanna G. The landscape of the mesenchymal signature in brain tumours. *Brain* 2019; **142**(4): 847-66.
18. Mastrella G, Hou M, Li M, et al. Targeting APLN/APLNR Improves Antiangiogenic Efficiency and Blunts Proinvasive Side Effects of VEGFA/VEGFR2 Blockade in Glioblastoma. *Cancer Res* 2019; **79**(9): 2298-313.

19. Quail DF, Joyce JA. The Microenvironmental Landscape of Brain Tumors. *Cancer Cell* 2017; **31**(3): 326-41.
20. Markovic DS, Vinnakota K, Chirasani S, et al. Gliomas induce and exploit microglial MT1-MMP expression for tumor expansion. *Proc Natl Acad Sci U S A* 2009; **106**(30): 12530-5.
21. Glass R, Synowitz M. CNS macrophages and peripheral myeloid cells in brain tumours. *Acta Neuropathol* 2014; **128**(3): 347-62.
22. Poon CC, Sarkar S, Yong VW, Kelly JJP. Glioblastoma-associated microglia and macrophages: targets for therapies to improve prognosis. *Brain* 2017; **140**(6): 1548-60.
23. Hambardzumyan D, Gutmann DH, Kettenmann H. The role of microglia and macrophages in glioma maintenance and progression. *Nat Neurosci* 2016; **19**(1): 20-7.
24. Muller S, Kohanbash G, Liu SJ, et al. Single-cell profiling of human gliomas reveals macrophage ontogeny as a basis for regional differences in macrophage activation in the tumor microenvironment. *Genome Biol* 2017; **18**(1): 234.
25. Zhu C, Kros JM, Cheng C, Mustafa D. The contribution of tumor-associated macrophages in glioma neo-angiogenesis and implications for anti-angiogenic strategies. *Neuro Oncol* 2017; **19**(11): 1435-46.
26. Lim M, Xia Y, Bettegowda C, Weller M. Current state of immunotherapy for glioblastoma. *Nat Rev Clin Oncol* 2018; **15**(7): 422-42.
27. Nduom EK, Weller M, Heimberger AB. Immunosuppressive mechanisms in glioblastoma. *Neuro Oncol* 2015; **17 Suppl 7**: vii9-vii14.
28. Stock K, Kumar J, Synowitz M, et al. Neural precursor cells induce cell-death of high-grade astrocytomas via stimulation of TRPV1. *Nature Medicine* 2012; **18**: 1232-8.
29. Hide T, Komohara Y, Miyasato Y, et al. Oligodendrocyte Progenitor Cells and Macrophages/Microglia Produce Glioma Stem Cell Niches at the Tumor Border. *EBioMedicine* 2018; **30**: 94-104.
30. Huang Y, Hoffman C, Rajappa P, et al. Oligodendrocyte progenitor cells promote neovascularization in glioma by disrupting the blood-brain barrier. *Cancer research* 2014; **74**(4): 1011-21.
31. Audia A, Conroy S, Glass R, Bhat KPL. The Impact of the Tumor Microenvironment on the Properties of Glioma Stem-Like Cells. *Frontiers in oncology* 2017; **7**: 143.
32. Crisan M, Yap S, Casteilla L, et al. A perivascular origin for mesenchymal stem cells in multiple human organs. *Cell stem cell* 2008; **3**(3): 301-13.
33. Winkler EA, Bell RD, Zlokovic BV. Central nervous system pericytes in health and disease. *Nat Neurosci* 2011; **14**(11): 1398-405.
34. Sweeney MD, Ayyadurai S, Zlokovic BV. Pericytes of the neurovascular unit: key functions and signaling pathways. *Nat Neurosci* 2016; **19**(6): 771-83.
35. Armulik A, Genove G, Betsholtz C. Pericytes: developmental, physiological, and pathological perspectives, problems, and promises. *Dev Cell* 2011; **21**(2): 193-215.
36. Lindahl P, Johansson BR, Leveen P, Betsholtz C. Pericyte loss and microaneurysm formation in PDGF-B-deficient mice. *Science* 1997; **277**(5323): 242-5.
37. Nehls V, Drenckhahn D. The versatility of microvascular pericytes: from mesenchyme to smooth muscle? *Histochemistry* 1993; **99**(1): 1-12.

38. Nehls V, Denzer K, Drenckhahn D. Pericyte involvement in capillary sprouting during angiogenesis in situ. *Cell Tissue Res* 1992; **270**(3): 469-74.
39. Dermietzel R, Krause D. Molecular anatomy of the blood-brain barrier as defined by immunocytochemistry. *Int Rev Cytol* 1991; **127**: 57-109.
40. Ruiter DJ, Schlingemann RO, Westphal JR, Denijn M, Rietveld FJ, De Waal RM. Angiogenesis in wound healing and tumor metastasis. *Behring Inst Mitt* 1993; (92): 258-72.
41. Hartmann DA, Underly RG, Grant RI, Watson AN, Lindner V, Shih AY. Pericyte structure and distribution in the cerebral cortex revealed by high-resolution imaging of transgenic mice. *Neurophotonics* 2015; **2**(4): 041402.
42. Etchevers HC, Vincent C, Le Douarin NM, Couly GF. The cephalic neural crest provides pericytes and smooth muscle cells to all blood vessels of the face and forebrain. *Development* 2001; **128**(7): 1059-68.
43. Korn J, Christ B, Kurz H. Neuroectodermal origin of brain pericytes and vascular smooth muscle cells. *J Comp Neurol* 2002; **442**(1): 78-88.
44. Kurz H. Cell lineages and early patterns of embryonic CNS vascularization. *Cell Adh Migr* 2009; **3**(2): 205-10.
45. Hellstrom M, Kalen M, Lindahl P, Abramsson A, Betsholtz C. Role of PDGF-B and PDGFR-beta in recruitment of vascular smooth muscle cells and pericytes during embryonic blood vessel formation in the mouse. *Development* 1999; **126**(14): 3047-55.
46. Abramsson A, Kurup S, Busse M, et al. Defective N-sulfation of heparan sulfate proteoglycans limits PDGF-BB binding and pericyte recruitment in vascular development. *Genes Dev* 2007; **21**(3): 316-31.
47. Kokovay E, Li L, Cunningham LA. Angiogenic recruitment of pericytes from bone marrow after stroke. *J Cereb Blood Flow Metab* 2006; **26**(4): 545-55.
48. Zhou W, Chen C, Shi Y, et al. Targeting Glioma Stem Cell-Derived Pericytes Disrupts the Blood-Tumor Barrier and Improves Chemotherapeutic Efficacy. *Cell Stem Cell* 2017; **21**(5): 591-603 e4.
49. Gautam J, Yao Y. Roles of Pericytes in Stroke Pathogenesis. *Cell Transplant* 2018; **27**(12): 1798-808.
50. Leal-Campanario R, Alarcon-Martinez L, Rieiro H, et al. Abnormal Capillary Vasodynamics Contribute to Ictal Neurodegeneration in Epilepsy. *Sci Rep* 2017; **7**: 43276.
51. Dias DO, Kim H, Holl D, et al. Reducing Pericyte-Derived Scarring Promotes Recovery after Spinal Cord Injury. *Cell* 2018; **173**(1): 153-65 e22.
52. Sagare AP, Bell RD, Zhao Z, et al. Pericyte loss influences Alzheimer-like neurodegeneration in mice. *Nat Commun* 2013; **4**: 2932.
53. Ferland-McCollough D, Slater S, Richard J, Reni C, Mangialardi G. Pericytes, an overlooked player in vascular pathobiology. *Pharmacol Ther* 2017; **171**: 30-42.
54. Sun H, Guo D, Su Y, et al. Hyperplasia of pericytes is one of the main characteristics of microvascular architecture in malignant glioma. *PLoS One* 2014; **9**(12): e114246.
55. Ginhoux F, Jung S. Monocytes and macrophages: developmental pathways and tissue homeostasis. *Nat Rev Immunol* 2014; **14**(6): 392-404.
56. Saijo K, Glass CK. Microglial cell origin and phenotypes in health and disease. *Nat Rev Immunol* 2011; **11**(11): 775-87.
57. Prinz M, Priller J. Microglia and brain macrophages in the molecular age: from origin to neuropsychiatric disease. *Nat Rev Neurosci* 2014; **15**(5): 300-12.

58. Prinz M, Erny D, Hagemeyer N. Ontogeny and homeostasis of CNS myeloid cells. *Nat Immunol* 2017; **18**(4): 385-92.
59. Badie B, Schartner JM. Flow cytometric characterization of tumor-associated macrophages in experimental gliomas. *Neurosurgery* 2000; **46**(4): 957-61; discussion 61-2.
60. Parney IF, Waldron JS, Parsa AT. Flow cytometry and in vitro analysis of human glioma-associated macrophages. Laboratory investigation. *J Neurosurg* 2009; **110**(3): 572-82.
61. Coniglio SJ, Eugenin E, Dobrenis K, et al. Microglial stimulation of glioblastoma invasion involves epidermal growth factor receptor (EGFR) and colony stimulating factor 1 receptor (CSF-1R) signaling. *Mol Med* 2012; **18**: 519-27.
62. Carvalho da Fonseca AC, Wang H, Fan H, et al. Increased expression of stress inducible protein 1 in glioma-associated microglia/macrophages. *J Neuroimmunol* 2014; **274**(1-2): 71-7.
63. Wick W, Platten M, Weller M. Glioma cell invasion: regulation of metalloproteinase activity by TGF-beta. *J Neurooncol* 2001; **53**(2): 177-85.
64. Chen X, Zhang L, Zhang IY, et al. RAGE expression in tumor-associated macrophages promotes angiogenesis in glioma. *Cancer Res* 2014; **74**(24): 7285-97.
65. Brandenburg S, Muller A, Turkowski K, et al. Resident microglia rather than peripheral macrophages promote vascularization in brain tumors and are source of alternative pro-angiogenic factors. *Acta Neuropathol* 2016; **131**(3): 365-78.
66. Veitenhansl M, Stegner K, Hierl FX, et al. 40(th) EASD Annual Meeting of the European Association for the Study of Diabetes : Munich, Germany, 5-9 September 2004. *Diabetologia* 2004; **47**(Suppl 1): A1-A464.
67. Feil S, Valtcheva N, Feil R. Inducible Cre mice. *Methods Mol Biol* 2009; **530**: 343-63.
68. Kos CH. Cre/loxP system for generating tissue-specific knockout mouse models. *Nutr Rev* 2004; **62**(6 Pt 1): 243-6.
69. Feil R. Conditional somatic mutagenesis in the mouse using site-specific recombinases. *Handb Exp Pharmacol* 2007; (178): 3-28.
70. Mignone JL, Kukekov V, Chiang AS, Steindler D, Enikolopov G. Neural stem and progenitor cells in nestin-GFP transgenic mice. *J Comp Neurol* 2004; **469**(3): 311-24.
71. Kulkarni S, Micci MA, Leser J, et al. Adult enteric nervous system in health is maintained by a dynamic balance between neuronal apoptosis and neurogenesis. *Proc Natl Acad Sci U S A* 2017; **114**(18): E3709-E18.
72. McLellan MA, Rosenthal NA, Pinto AR. Cre-loxP-Mediated Recombination: General Principles and Experimental Considerations. *Curr Protoc Mouse Biol* 2017; **7**(1): 1-12.
73. Zhang S, Zhu X, Gui X, et al. Sox2 Is Essential for Oligodendroglial Proliferation and Differentiation during Postnatal Brain Myelination and CNS Remyelination. *J Neurosci* 2018; **38**(7): 1802-20.
74. Brockschnieder D, Pechmann Y, Sonnenberg-Riethmacher E, Riethmacher D. An improved mouse line for Cre-induced cell ablation due to diphtheria toxin A, expressed from the Rosa26 locus. *Genesis* 2006; **44**(7): 322-7.

75. Yona S, Kim KW, Wolf Y, et al. Fate mapping reveals origins and dynamics of monocytes and tissue macrophages under homeostasis. *Immunity* 2013; **38**(1): 79-91.
76. Arinobu Y, Mizuno S, Chong Y, et al. Reciprocal activation of GATA-1 and PU.1 marks initial specification of hematopoietic stem cells into myeloerythroid and myelolymphoid lineages. *Cell Stem Cell* 2007; **1**(4): 416-27.
77. Smith AM, Gibbons HM, Oldfield RL, et al. The transcription factor PU.1 is critical for viability and function of human brain microglia. *Glia* 2013; **61**(6): 929-42.
78. Goldmann T, Wieghofer P, Jordao MJ, et al. Origin, fate and dynamics of macrophages at central nervous system interfaces. *Nat Immunol* 2016; **17**(7): 797-805.
79. Nutt SL, Metcalf D, D'Amico A, Polli M, Wu L. Dynamic regulation of PU.1 expression in multipotent hematopoietic progenitors. *J Exp Med* 2005; **201**(2): 221-31.
80. Buza-Vidas N, Woll P, Hultquist A, et al. FLT3 expression initiates in fully multipotent mouse hematopoietic progenitor cells. *Blood* 2011; **118**(6): 1544-8.
81. Boiers C, Buza-Vidas N, Jensen CT, et al. Expression and role of FLT3 in regulation of the earliest stage of normal granulocyte-monocyte progenitor development. *Blood* 2010; **115**(24): 5061-8.
82. Brown CR, Reiner SL. Bone-marrow chimeras reveal hemopoietic and nonhemopoietic control of resistance to experimental Lyme arthritis. *J Immunol* 2000; **165**(3): 1446-52.
83. Antoine Louveau JK. Dissection and meninges of mouse whole-mount meninges. 2015 (accessed 2 June 2015 2015).
84. Wittekind D. Traditional staining for routine diagnostic pathology including the role of tannic acid. 1. Value and limitations of the hematoxylin-eosin stain. *Biotechnic & Histochemistry* 2003; **78**(5): 261-70.
85. Price RL, Jerome WG. Basic confocal microscopy. New York: Springer; 2011.
86. Cheng L, Huang Z, Zhou W, et al. Glioblastoma stem cells generate vascular pericytes to support vessel function and tumor growth. *Cell* 2013; **153**(1): 139-52.
87. Kovacs GG. Cellular reactions of the central nervous system. *Handb Clin Neurol* 2017; **145**: 13-23.
88. Hammond TR, Robinton D, Stevens B. Microglia and the Brain: Complementary Partners in Development and Disease. *Annual review of cell and developmental biology* 2018; **34**: 523-44.
89. Armulik A, Genove G, Mae M, et al. Pericytes regulate the blood-brain barrier. *Nature* 2010; **468**(7323): 557-61.
90. Jones E, Schafer R. Where is the common ground between bone marrow mesenchymal stem/stromal cells from different donors and species? *Stem Cell Res Ther* 2015; **6**: 143.
91. Graham V, Khudyakov J, Ellis P, Pevny L. SOX2 functions to maintain neural progenitor identity. *Neuron* 2003; **39**(5): 749-65.
92. Sarkar A, Hochedlinger K. The sox family of transcription factors: versatile regulators of stem and progenitor cell fate. *Cell Stem Cell* 2013; **12**(1): 15-30.
93. Serbina NV, Hohl TM, Cherny M, Pamer EG. Selective expansion of the monocytic lineage directed by bacterial infection. *J Immunol* 2009; **183**(3): 1900-10.

94. Kierdorf K, Erny D, Goldmann T, et al. Microglia emerge from erythromyeloid precursors via Pu.1- and Irf8-dependent pathways. *Nat Neurosci* 2013; **16**(3): 273-80.
95. Mouton PR, Gokhale AM, Ward NL, West MJ. Stereological length estimation using spherical probes. *J Microsc* 2002; **206**(Pt 1): 54-64.
96. Mathivet T, Bouleti C, Van Woensel M, et al. Dynamic stroma reorganization drives blood vessel dysmorphia during glioma growth. *EMBO Mol Med* 2017; **9**(12): 1629-45.
97. Bifari F, Berton V, Pino A, et al. Meninges harbor cells expressing neural precursor markers during development and adulthood. *Front Cell Neurosci* 2015; **9**: 383.
98. Glass R, Synowitz M, Kronenberg G, et al. Glioblastoma-induced attraction of endogenous neural precursor cells is associated with improved survival. *J Neurosci* 2005; **25**(10): 2637-46.
99. Simonavicius N, Robertson D, Bax DA, Jones C, Huijbers IJ, Isacke CM. Endosialin (CD248) is a marker of tumor-associated pericytes in high-grade glioma. *Mod Pathol* 2008; **21**(3): 308-15.
100. Balabanov R, Washington R, Wagnerova J, Dore-Duffy P. CNS microvascular pericytes express macrophage-like function, cell surface integrin alpha M, and macrophage marker ED-2. *Microvasc Res* 1996; **52**(2): 127-42.
101. Chen Z, Feng X, Herting CJ, et al. Cellular and Molecular Identity of Tumor-Associated Macrophages in Glioblastoma. *Cancer Res* 2017; **77**(9): 2266-78.
102. Umekawa T, Osman AM, Han W, Ikeda T, Blomgren K. Resident microglia, rather than blood-derived macrophages, contribute to the earlier and more pronounced inflammatory reaction in the immature compared with the adult hippocampus after hypoxia-ischemia. *Glia* 2015; **63**(12): 2220-30.
103. Guimaraes-Camboa N, Cattaneo P, Sun Y, et al. Pericytes of Multiple Organs Do Not Behave as Mesenchymal Stem Cells In Vivo. *Cell Stem Cell* 2017; **20**(3): 345-59 e5.
104. Kueh HY, Champhekar A, Nutt SL, Elowitz MB, Rothenberg EV. Positive feedback between PU.1 and the cell cycle controls myeloid differentiation. *Science* 2013; **341**(6146): 670-3.
105. Tosic N, Petrovic I, Grujicic NK, et al. Prognostic significance of SOX2, SOX3, SOX11, SOX14 and SOX18 gene expression in adult de novo acute myeloid leukemia. *Leuk Res* 2018; **67**: 32-8.
106. Muller A, Brandenburg S, Turkowski K, Muller S, Vajkoczy P. Resident microglia, and not peripheral macrophages, are the main source of brain tumor mononuclear cells. *Int J Cancer* 2015; **137**(2): 278-88.
107. Sarkar S, Doring A, Zemp FJ, et al. Therapeutic activation of macrophages and microglia to suppress brain tumor-initiating cells. *Nature neuroscience* 2014; **17**(1): 46-55.
108. Liu Z, Kuang W, Zhou Q, Zhang Y. TGF-beta1 secreted by M2 phenotype macrophages enhances the stemness and migration of glioma cells via the SMAD2/3 signalling pathway. *Int J Mol Med* 2018; **42**(6): 3395-403.
109. Rosager AM, Sorensen MD, Dahlrot RH, et al. Expression and prognostic value of JAM-A in gliomas. *Journal of neuro-oncology* 2017; **135**(1): 107-17.

8. Acknowledgements

Firstly, I would like to express my deep gratitude to Professor Rainer Glaß, my doctoral supervisor, for his patient guidance, enthusiastic encouragement and useful critiques of my studies. His broad knowledge empowered me with good solutions to solve difficult problems. His strong motivation for the truth of the real world encourages me always. He respects and trusts me. He gave me these interesting and challenging scientific projects. His kindness and noble personality impact me a lot. Words are powerless to express my gratitude to him!

Secondly, I would like to acknowledge supports and constructive advice from Dr. Roland Kälin with much appreciation. I am particularly thankful to Ms. Stefanie Lange, for her kindly helps. Assistance provided by Ms..Cheng Jiying is also greatly appreciated. Moreover, many thanks to all colleagues of the Neurosurgical Research, Dr. Wu Yingxi, Mr. Li Min, Dr. Marie Nhery Murielle Volmar, Dr. Li Yuping, Dr. Gu Song, Mr. Hou Mengzhuo, Dr. Giorgia Mastrella, Mr. Zhao Dongxu, Mr Philipp Graeff, Mr. Zhang Huabin, Dr. Ramazan Uyar, Ms. Lisa Niederauer, Ms. Nina Zdouc, Mr. Rafael Leite, Mr. Haitam Alenezi, Mr. Barci Enio, Mr. Sven Richter, and Ms. Lena Schumacher. My special thanks extend to Ms. Birgit Blechert and Dr Franz Schilling, from the basic science laboratory of the Department of Nuclear Medicine at the Technical University in Munich. I also appreciate all our collaborators and all technicians, Mr Zhang Wenlong, Dr Andreas Thomae et al.

Furthermore, I want to acknowledge directions from my mentor Professor Yuan Xianrui. Also, I am grateful for the encouragement of Professor Chen Qianxue, Dr. Jian Zhihong and Professor Li Mingchang. China Scholarship Council is also appreciated for providing me the financial support.

Last but not least, I would also like to thank my family for their endless love and support. Thanks to Yawen, my mother, my father, my grandfather and my departed grandmother! With their love, I got persistence, dedication, forbearance and a steady temper. I love them and I am proud of them!